5. Clocks

Ron Beard, Ken Senior

This chapter provides an overview of clock technology and typical clocks (Cs, Rb, H-Maser) in use today for onboard and ground systems and identifies future trends such as fountain clocks, etc. Concepts such as clock drift, trend, random variations and the statistical methods for their characterization (Allan deviation (ADEV), etc.) are introduced and performance characteristics of global navigation satellite system (GNSS) onboard clocks are presented. The handling and impact of special and general relativity on timing measurements are discussed. Finally, the generation of a GNSS time from an ensemble of ground clocks is described.

Today's time and frequency standards range from the most sophisticated reference standards to the smallest oscillators for handheld radios. The technical requirements and technologies needed are different for the various applications but they derive from similar physical concepts. These different technologies can be categorized into four major areas: reference standards, mobile systems, handheld and space systems. These areas are the core areas of time and frequency standard applications and different areas of technology are needed to address them.

Clocks and oscillators are needed by reference timescale centers such as those that contribute to the international time scale, Universal Time Coordinated (UTC). This specialized area requires the most highly stable and accurate time standards that are maintained under controlled environmental conditions. Their outputs are processed with special ensembling algorithms designed to produce an absolute reference for all systems. For example, the current suite of clocks used at the US Naval Observatory (USNO) consists of many commercial cesium beam frequency standards and hydrogen masers, and specially built rubidium fountain standards. These clocks are physically separated and operated in a tightly controlled environment. Size, weight and power are not issues pertinent for these clocks; primary emphasis is on performance, mostly for intervals of days and much longer.

Clocks used in mobile applications are typically crystal oscillator-based devices and small atomic clocks or oscillators used for positioning, communications or internal to other remote sensing systems. The requirements for mobile devices typically emphasize size, weight and power rather than time and frequency performance so their performance requirements are not particularly demanding or rigorous.

Devices used in handheld applications are the most demanding in terms of size, weight and power. They

commonly use small quartz crystal oscillators. However, in recent years there have been several efforts to develop extremely small atomic standards. These small atom standards offer better accuracy and stability than crystal oscillators in an extremely small package. Although their performance exceeds that of crystal oscillator-based devices they have yet to perform as well as their larger mobile or timing center devices, although there are efforts underway to attempt to improve performance. The technologies developed for these devices have benefited from development in atomic interrogation different from that used by the conventional commercial standards and will be described later.

Space-qualified atomic standards constitute a unique class of frequency standards next to ground- or aircraft-based standards. They were essential for the development and deployment of global navigation satellite systems (GNSS), which are currently the dominant user of highly precise and stable space-qualified atomic standards. These types of standards provide high stability for navigation performance and a large part of the development of these space devices has been to reliably provide high stability. The GNSS user receiving equipment and the timing capability resulting from their use of the atomic standards in the GNSS satellites produce an inexpensive alternative to high-precision atomic clocks. By displacing higher cost, higher performing atomic clocks, GNSS user equipment receivers or timing receivers with low quality clocks are being deployed in a wide variety of systems. For example, naval tactical and strategic systems are currently utilizing hundreds of Global Positioning System (GPS) units, which are displacing systems on larger ships that may have previously used multiple cesium beam standards on board. Secondary standards such as rubidium vapor cell and crystal oscillators are being used extensively in aircraft, shipboard and man-portable applications, since virtually every system has a clock or oscillator of some quality contained in it.

5.1 Frequency and Time Stability

The oscillator is the basic unit on which clocks, timekeeping and timescales are founded. The fundamental relationship between frequency and time is

$$f = \frac{1}{\tau} , \tag{5.1}$$

where f is the frequency of the oscillator, and the period τ is the time interval that a clock uses for time keeping. A clock mechanism added to an oscillator accumulates or counts the number of time intervals to measure elapsed time thereby generating a clock. The intimate connection between oscillators and clocks is sometimes confused by calling a clock a frequency standard or vice versa. A generic clock system is illustrated in Fig. 5.1.

However, oscillators are not perfect and various types have been developed for different requirements and applications. The determination of oscillator or clock performance under different conditions ranging from ideal laboratory conditions, to harsh field environments, such as military field radios, is an area of special concern.

Oscillators or frequency sources produce noise that appears to be a superposition of causally generated signals and random, nondeterministic noises. Random noises include thermal noise, shot noise, and noises of undetermined origin, such as flicker noise. The end result is time-dependent phase and amplitude fluctuations. Measurement of these fluctuations can be used to characterize the oscillator in terms of amplitude modulation (AM) and phase modulation (PM) noise, and the combination is more commonly called frequency stability. This section describes the basic concepts and measures used to describe the frequency and time stability of precision clocks.

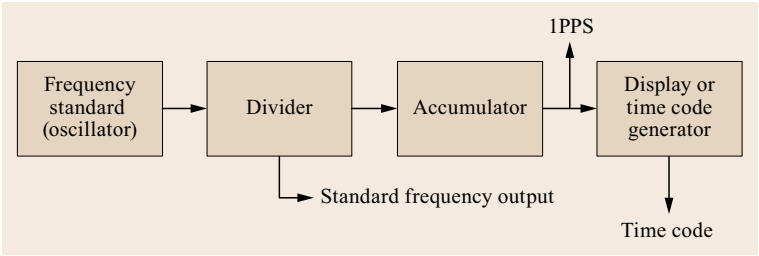

Fig. 5.1 Generic clock system

5.1.1 Concepts

Frequency stability encompasses the concept of random noise, intended and incidental noise, and any other fluctuations in the output frequency of a device. In general, frequency stability is the degree to which an oscillator produces the same frequency throughout a specified period of time. It is implicit in this general definition that the stability of a given frequency decreases if it is anything except a perfect sine wave.

The oscillator produces a signal, whose voltage output may be written as,

$$V(t) = [V_0 + \varepsilon(t)] \sin [2\pi \nu_0 t + \phi(t)] \ ,$$

where V_0 is the nominal peak voltage amplitude, ν_0 is the nominal fundamental frequency, and where $\varepsilon(t)$ and $\phi(t)$ represent the fluctuations in amplitude and phase of the oscillator from their nominal value, and t represents elapsed time. The instantaneous angular frequency of the oscillator is defined as the time derivative of its total phase

$$\omega(t) = \frac{\mathrm{d}}{\mathrm{d}t} [2\pi \nu_0 t + \phi(t)]$$

and therefore its instantaneous frequency as $\nu(t) = \omega(t)/(2\pi)$, or

$$\nu(t) = \nu_0 + \frac{1}{2\pi} \frac{\mathrm{d}\phi}{\mathrm{d}t} \ . \tag{5.2}$$

For precision oscillators the amplitude fluctuations ε may generally be neglected as they are usually very small compared to the nominal amplitude and therefore have no substantial influence on the frequency or phase. Also, the second term of (5.2) is quite small as compared to the nominal frequency ν_0 and so it is more convenient to define the normalized (or factional) frequency as

$$y(t) = \frac{\nu(t) - \nu_0}{\nu_0} = \frac{1}{2\pi \nu_0} \frac{\mathrm{d}\phi}{\mathrm{d}t} \ , \tag{5.3}$$

which is unitless and which may also be used as a basis for comparing oscillators operating at nominally different frequencies. The phase may then be expressed in units of time as

$$x(t) = \frac{\phi(t)}{2\pi \nu_0} \ , \tag{5.4}$$

that is,

$$y(t) = x'(t) \ .$$

A generally applicable model of the time error of a clock, $T(t)$, at an elapsed time, t, after synchronization with another, presumably better clock, can be expressed as

$$T(t) = x_0 + y_0 t + \frac{1}{2} D_0 t^2 + \int_0^t E(t)\mathrm{d}t + \varepsilon(t) \ , \tag{5.5}$$

where x_0 represents the synchronization error or offset at $t = 0$, y_0 represents a constant rate or frequency offset of the clock and D_0 represents a constant frequency drift, and $\varepsilon(t)$ represents all the random deviations of the clock's error. The quantity $E(t)$ represents any remaining systematic nonconstant rate difference due to environmental effects (temperature, radiation, accelerations, etc.).

Although the environmental effects are not usually explicitly modeled such effects can be large and should not be ignored especially in field or operating systems. The random fluctuations are often concentrated upon since they may be measured by statistical means after the systematic components, x_0, y_0, and D_0 are removed from the clock data. Characterization of the clock's random error contribution to its total time or frequency error is the subject of the next section on stability.

5.1.2 Characterization of Clock Stability

While no single formal definition of stability exists, the characterization of the stability of a clock may be generally considered as any quantification of the stability of the time and frequency output of the device. A number of different measures of stability have been developed over the years to characterize clocks and numerous papers have been published in more detail than presented here. In particular, the information presented here does not include the various methods and special considerations for measuring clocks and oscillators. For a more comprehensive treatment of the characterization methodology refer to the collection of papers in [5.1], and more recent publications [5.2–5].

In an attempt to make uniform the specifications of clocks through the characterization of their stability the Institute of Electrical and Electronic Engineers (IEEE) in the 1970s made several recommended measures of stability, which can broadly be separated into two analysis areas: sample time-averaged or time domain methods and Fourier spectral or frequency domain methods [5.6]. Both approaches may be related mathematically as shown below, though historically either approach was utilized because the particular methods for measuring clocks' error dictated one method over the other. With the progress in digital processing since

the 1960s both methods can usually be applied for clocks measured today [5.7].

The IEEE has recommended as its primary frequency domain measure of a clock's stability the one-sided spectral density $S_y(f)$ of its fractional frequency, or of its spectral density of phase $S_x(f)$ (or $S_\phi(f)$), which, by properties of derivatives and the Fourier transform, are related by

$$S_y(f) = \left(\frac{f}{\nu_0}\right)^2 ,$$
$$S_\phi(f) = (2\pi f)^2 S_x(f) . \tag{5.6}$$

Here note that f represents the Fourier frequency, which should be distinguished from the frequency output of the clock, ν (or y).

The spectral density $S_x(f)$ may be calculated from observations of its corresponding phase or time signal $x(t)$ by using Fourier transforms. The relationship between the Fourier transform $X(f)$ of the signal and the signal itself is given by

$$X(f) = \int_{-\infty}^{\infty} x(t) \mathrm{e}^{-2\pi \mathrm{j} f t} \mathrm{d}t . \tag{5.7}$$

However, not all the measurements of $x(t)$ are practically available at all continuous values of t. Given evenly spaced discrete measurements $x(k\tau_0)$ of x, where τ_0 is the smallest sampling interval, and k is an integer, the discrete Fourier transform may be invoked where the integral is replaced by an infinite sum

$$X(f) = \sum_{k=-\infty}^{+\infty} x(k\tau_0) \mathrm{e}^{-2\pi \mathrm{j} f} . \tag{5.8}$$

If the timing signals are assumed to be periodic, that is $x(t+T) = x(t)$ for all t and some period T, then its Fourier series is also discrete.

Assuming together that the signal x is periodic with period T and there are N evenly spaced phase measurements $x(k\tau_0)$, such that $N\tau_0 = T$, the Fourier series at a finite number of Fourier frequencies may be calculated using just a finite sum

$$X\left(\frac{n}{N\tau_0}\right) = \sum_{k=0}^{N-1} x(k\tau_0) \mathrm{e}^{-2\pi \mathrm{j}(kn/N)} \tag{5.9}$$

for each $n = 0, 1, \ldots, N-1$. In other words, the full Fourier frequency content occurs at an exact finite number of frequencies $f_n = n/(N\tau_0)$ with smallest nonzero Fourier frequency f_1 and largest frequency f_{N-1}. Any Fourier frequency content occurring at frequencies larger than the Nyquist frequency $(1/(2\tau_0))$, or half the sampling frequency) or content in violation of the periodicity assumption will alias into the spectrum calculated from (5.9).

The spectral density of phase (time) may be calculated from (5.9) by combining the squares of the real and imaginary components and dividing by the total time interval T

$$S_x(f_n) = \frac{\mathrm{Re}\{X(f_n)\}^2 + \mathrm{Im}\{X(f_n)\}^2}{T} . \tag{5.10}$$

A generally applicable model for the random fluctuations of most clocks describes the spectral density of phase as a sum of seven independent pure power laws up to a limiting frequency

$$S_x(f) = \begin{cases} \sum_{\beta=-6}^{0} g_\beta f^\beta & \text{for } 0 < f < f_\mathrm{h} \\ 0 & \text{for } f_\mathrm{h} < f . \end{cases} \tag{5.11}$$

Here, β are integers, the g_β are constants indicating the spectral level of the noise, and f_h is the high frequency cutoff of a low-pass filter. The high frequency cutoff is necessary since variances involving integration of $S_x(f)$ over f would yield unrealistic infinite energies. Also, it is assumed that only integer values of β may be present as the model was mostly empirically derived. For an excellent treatment of the continuous β case see [5.4].

Figure 5.2 shows the phase fluctuations of five simulated clocks having spectral densities of phase, $S_x(f) \sim f^\beta$ for $\beta = 0, -1, -2, -3$, and -4. $\beta = -5$ and -6 were not included since their variations would outscale the other series in the plot. Note that although the series in the figure show realizations of each power law independently a clock may consist of any or all of the processes simultaneously as per the sum in (5.11). These common clock pure power-law noises are often referred to as white phase noise (WHPH, f^0), flicker phase (FLPH, f^{-1}), random walk phase (RWPH, f^{-2}), flicker frequency (FLFR, f^{-3}), random walk frequency (RWFR, f^{-4}), flicker drift (FLDR, f^{-5}), and random walk drift (RWDR, f^{-6}). It is usually the case that one of the noise processes will dominate at a given Fourier frequency so that a plot of Fourier frequency f versus the logarithm of spectral density of phase $S_x(f)$ would indicate the β noise type that is dominant.

Several time-domain or time-averaged measures have been recommended by the IEEE for characterization of stability. The most well-known measure is the two-sample variance (or Allan variance) for quantify-

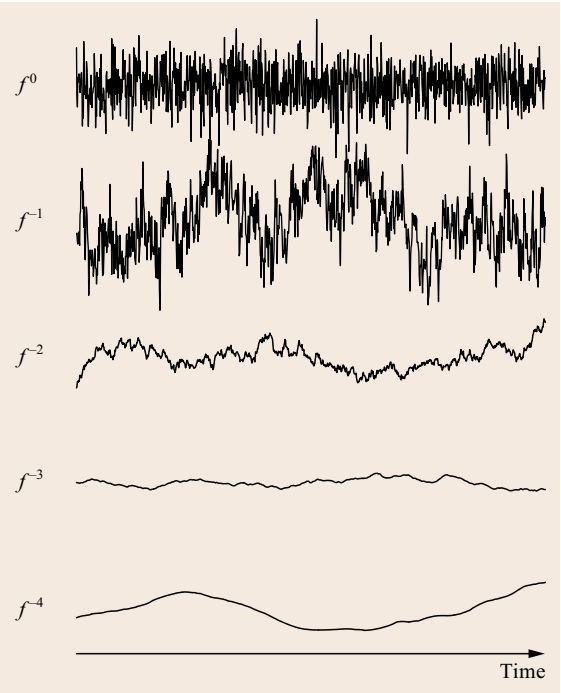

Fig. 5.2 Example simulated realizations of phase (time) fluctuations of five random processes each having respectively from top to bottom spectral densities of phase, $S_x(f) \sim f^\beta$ for $\beta = 0, \ldots, -4$

ing frequency stability. It is defined as

$$\sigma_y^2(\tau) = \left\langle \frac{(\bar{y}_{k+1} - \bar{y}_k)^2}{2} \right\rangle , \tag{5.12}$$

where $\langle\cdot\rangle$ denotes infinite time average (or expectation) and where

$$\bar{y}_k = \frac{1}{\tau} \int_{t_k}^{t_k+\tau} y(t)\mathrm{d}t = \frac{x_{k+1} - x_k}{\tau}$$

is the average fractional frequency over the interval $\tau = t_{k+1} - t_k$. It is assumed in this definition that the average frequency values are adjacent, that is, no dead time exists between the phase measurement samples x_k. If dead time exists between the samples the resulting calculations will be biased such that the result is no longer considered the Allan variance. The Allan variance is insensitive to an overall systematic frequency or rate offset, y_0, because fractional frequency averages are differenced in (5.12).

The Allan variance is actually a special case ($N = 2$) of the more general classical N-sample variance,

$$\sigma_y^2(N, \tau) = \left\langle \frac{1}{N-1} \sum_{i=1}^{N} \left(\bar{y}_i - \sum_{j=1}^{N} \bar{y}_j \right)^2 \right\rangle , \tag{5.13}$$

which is an infinite time average of the variance of the N-sample mean of fractional frequency averages. One advantage of the two-sample variance over the N-sample variance is that (5.12) is a well-defined (finite) value for most of the power-law processes in (5.11) (namely for $\beta >= -4$). Expression (5.13), in contrast, diverges as $N \to \infty$ for $\beta < 0$ since it depends on the sample interval length T.

Another advantage of the Allan variance is that for power-law processes $\beta = 0, -1, \ldots, -4$ in (5.11) the Allan variance $\sigma_y^2(\tau)$ has a τ-relationship similar to the relationship of f to $S_x(f)$. In particular $\sigma_y^2(\tau) \sim |\tau|^\mu$, where $\mu = -3 - \beta$ for $\beta = -2, -3, -4$, while $\mu = -2$ for both $\beta = 0$ and $\beta = -1$. Thus on a log-log plot of τ versus $\sigma_y^2(\tau)$ the slope of the Allan variance curve can be used to indicate the type of noise dominant over that τ interval, except for the WHPH and FLPH noises, which have the same slope τ-Allan variance relationship.

Although the definition of the Allan variance is based on infinite time averaging, a means of estimating it from only a finite portion of the clock's phase realization is required in practice. A common formula used to estimate (5.12) utilizing N discrete samples of the average fractional frequency (or $M = N + 1$ phase samples) is

$$\sigma_y^2(\tau) \approx \frac{1}{2(N-1)} \sum_{i=1}^{N-1} (\bar{y}_{i+1} - \bar{y}_i)^2 \tag{5.14}$$

$$= \frac{1}{2(M-2)\tau^2} \sum_{i=1}^{M-2} (x_{i+2} - 2x_{i+1} + x_i)^2 . \tag{5.15}$$

An example clock realization of phase fluctuations is shown in Fig. 5.3, where $N+1$ measured phase samples are labeled and used to calculate the N average frequencies for a given interval τ. Confidence limits on the variance estimates of (5.14) and (5.12) must also be considered. As in the case of the spectral methods, the estimates obtained are highly dependent on the band-limiting elements of the measurement system. This includes the low-pass filter, which may not be specified as having a sharp cutoff frequency f_h, as assumed in the definition above [5.3].

Confidence limits can be improved by utilizing overlapping samples in the Allan variance calculation. However, the determination of confidence limits is

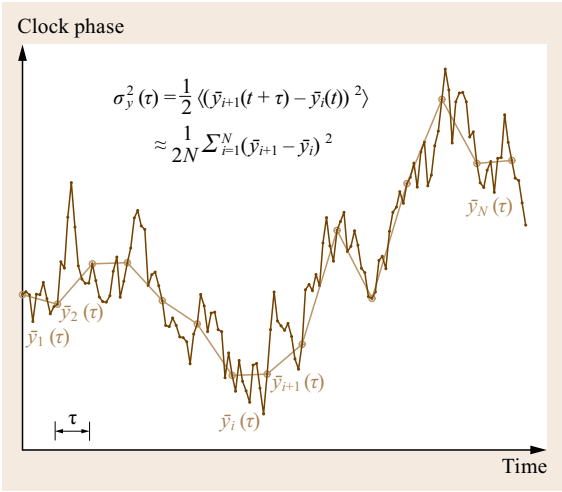

Fig. 5.3 Example of estimating the two-sample (Allan) variance for a given discrete series of clock phase measurements

more complex in this case, since the overlapping fractional frequency samples are no longer independent as in the nonoverlapping case. An estimate of the Allan variance calculated using all possible overlapped $\bar{y}$ samples may be written as

$$\sigma_y^2(\tau) \approx \frac{1}{2m^2(N-2m+1)} \times \sum_{j=1}^{N-2m+1}\left[\sum_{i=j}^{j+m-1}(\bar{y}_{i+1} - \bar{y}_i)\right]^2 . \quad (5.16)$$

Most manufacturers of precision clocks or oscillators as well as timing laboratories now routinely publish their clock stability specifications or performances using the Allan variance (or its square root, the Allan deviation). While the Allan variance may be the most widely used measure of frequency stability there are situations where spectral measures might be preferred. The following formula shows the relationship between the Allan variance and spectral density of phase [5.4]

$$\sigma_y^2(\tau) = \int_0^\infty 2S_x(f)\sin^4(\pi\tau f)\mathrm{d}f . \quad (5.17)$$

It is valid for all (continuous) $\beta > -5$ and shows that the Allan variance has a very broad Fourier response to energies that are purely harmonic. In this case a spectral approach is preferred over the Allan variance as any such bright lines are more easily identified with frequency domain techniques.

Other time-domain measures of stability include the modified Allan variance, $\mathrm{mod}\,\sigma_y^2(\tau)$, and the Hadamard variance. The modified Allan variance was introduced in order to address the deficiency of the Allan variance in distinguishing between WHPH and FLPH noises. It does so by effectively varying the (software) bandwidth of the variance calculation to establish the additional τ sensitivity. The Hadamard variance provides yet another time domain measure that converges for all the power-law processes in (5.11) and is insensitive to both an overall systematic rate, y_0, as well as an overall systematic drift D_0. Definitions of these variances along with the approximating formulas may be found in [5.1] and [5.5]. Because frequency stability values are commonly expressed as either Allan or Hadamard variances the relationship between the spectral density of phase and these statistics is shown in Table 5.1 for several of the common noise types.

Table 5.1 Relationship between the spectral density of phase $S_x(f)$, the Allan variance $\sigma_y^2(\tau)$, and the Hadamard variance $\mathrm{H}\sigma_y^2(\tau)$ for several common power-law noises

Noise name	Spectral density of phase	Allan variance	Hadamard variance
WHPH	g_0	$\tau^2\sigma_y^2(\tau)/(3f_\mathrm{h})$	$3\tau^2\mathrm{H}\sigma_y^2(\tau)/(10f_\mathrm{h})$
RWPH	$g_{-2}f^{-2}$	$\tau\sigma_y^2(\tau)$	$\tau\mathrm{H}\sigma_y^2(\tau)$
RWFR	$g_{-4}f^{-4}$	$3\sigma_y^2(\tau)/\tau$	$6\mathrm{H}\sigma_y^2(\tau)/\tau$
RWDR	$g_{-6}f^{-6}$	$20\sigma_y^2(\tau)/\tau^3$	$120\mathrm{H}\sigma_y^2(\tau)/(11\tau^3)$

5.2 Clock Technologies

As introduced in the previous section, clocks are based on oscillators that generate a periodic signal of a given frequency. The stability of this frequency and the resulting time count depends on the underlying physical principals and design properties and may vary widely between different classes of oscillators.

Key types of oscillators presented in this section include quartz crystal oscillators as well as cesium, rubidium, and hydrogen maser atomic clocks, which constitute the conventional atomic clock technology available today. An overview of the stability that can be expected from the different clock types is shown in Fig. 5.4.

5.2.1 Quartz Crystal Oscillators

The most common and ubiquitous oscillators available are those made with quartz crystals [5.8]. They are a basic form of harmonic oscillator beyond the simple electronic oscillators based on resistor-capacitor (RC) and inductor-capacitor (LC) circuits. Crystal oscillators are used in many forms of electronics and all GNSS receiving equipment operates with these devices to provide the necessary frequencies for radio frequency (RF) signal processing and to form an actual clock.

Quartz is a piezoelectric crystal material that can produce electrical signals by mechanical deformation of the material. Conversely, electrical signals can produce mechanical deformation [5.9]. Crystal oscillators have a higher quality factor (i. e., ratio of resonance frequency and resonance bandwidth) than the simpler RC and LC circuitry. They have better temperature stability but do use some of the same circuit designs as the LC oscillators with a quartz resonator replacing the tuned circuit portion. Other types of piezoelectric resonators use a surface acoustic waves (SAWs) mechanism, where the signals travel along the surface of the crystal material rather than the more traditional bulk acoustic wave (BAW) mechanism, in which the signals propagate through the crystal. Other types of physically mechanical oscillators are implemented with micro-electro-mechanical system (MEMS) techniques that use devices made from silicon processed through microelectronic fabrication techniques. The advantage in the MEMS devices is that they are simpler to manufacture and more compatible with modern microelectronic circuitry.

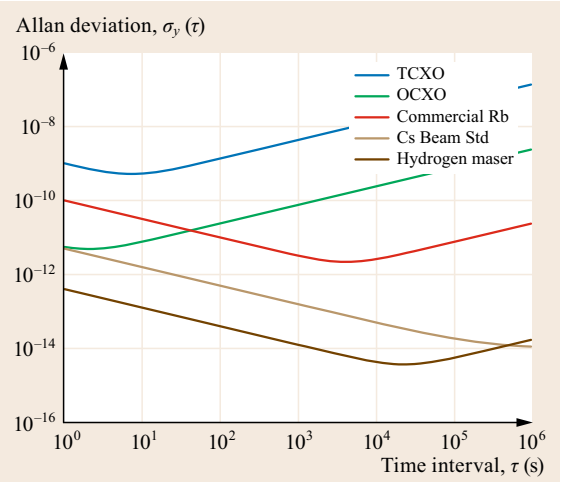

Fig. 5.4 Performance of the classical microwave atomic frequency standards compared with temperature-compensated (TCXOs) and oven-controlled (OCXOs) crystal oscillators

Crystal resonators are available to cover frequencies from about 1 kHz to over 200 MHz. At the low frequency end, wristwatch and real-time clock applications operate at 32.768 kHz and powers of two times this frequency. The conventional BAW resonators range from 80 kHz to 200 MHz. The frequencies of SAW devices range from above 50 MHz to the low GHz range.

The quartz crystal material is comprised of silicon dioxide and can occur naturally or can be grown synthetically. Oscillators are cut from these crystals in a variety of shapes. The shape, size and orientation within the crystalline structure determines the mode of vibration, its resonant frequency and properties of the oscillator. A voltage applied to the crystal will cause it to vibrate and produce a steady signal dependent upon the way the crystal is cut [5.10]. The process of making a quartz oscillator is very involved and complicated requiring material selection, cutting, polishing, mounting electrical contacts and sealing within an vacuum enclosure. Examples of 5 MHz fifth overtone oscillators are shown in Fig. 5.5 without the vacuum enclosure surrounding the crystal. These crystals are mounted on the contacts that extend through the vacuum enclosure to the electrodes plated on the crystal itself.

The quality of a crystal oscillator is determined by its frequency accuracy, frequency stability, aging effects and environmental effects. The absolute frequency accuracy of a crystal oscillator is between 10^{-6} and 10^{-7} taking into account environmental effects such as temperature, mechanical shock and aging. Stability can range from 10^{-10} to 10^{-12} depending upon how protected the crystal is from environmental variations. Aging is defined as the slow change in frequency over a period of time that is associated with long-term changes in the crystal itself or more dominant effects

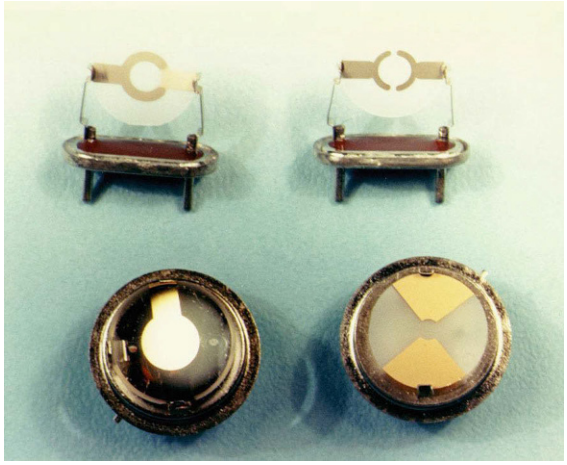

Fig. 5.5 Mounted crystal oscillators with different electrodes. Image courtesy of NRL

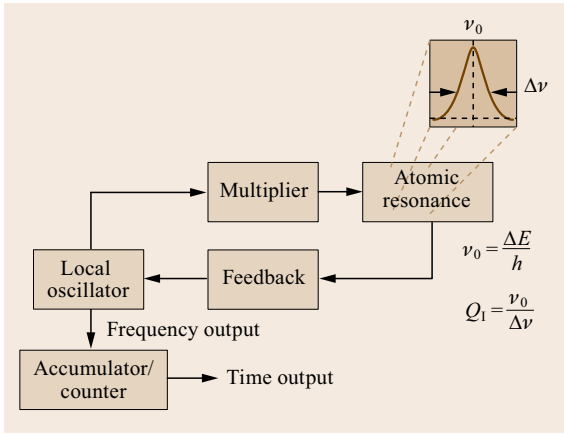

Fig. 5.6 Generic atomic standard block diagram

such as redistribution of contamination within the vacuum enclosure, slow leaks, mounting and electrode stresses that are relieved with time, and changes in atmospheric pressure. Environmental effects usually have a direct effect on the crystal such as thermal transients, mechanical vibration, shock, radiation, turning the crystal over (tip-over), magnetic fields, voltage changes and variations in the amount of power dissipated in the crystal.

The types of crystal cuts and the method of mitigating the environmental effects on the crystal determines the category of the oscillator. Three configurations in most common use are the room-temperature crystal oscillator (RTXO), the temperature-compensated crystal oscillator (TCXO), and the oven-controlled crystal oscillator (OCXO). The RTXO typically uses a hermetically sealed crystal and individual components for the oscillator circuit. The TCXO encloses the crystal, temperature-compensating components and the oscillator circuit in a container. The OCXO adds heater elements and controls to the oscillator circuit and encloses all the temperature-sensitive components in a thermally insulated container [5.10].

The increased demand for small-scale electronics for cell phones, portable entertainment electronics and miniaturized portable computers has stimulated the development of small-scale quartz oscillators, tuning forks and MEMS oscillators fabricated in silicon. MEMS resonator vibration is based on electrostatic dynamics rather than piezoelectric properties and the MEMS components are micromachined from silicon. They are configured in different complicated shapes such as combs, beam webs, discs and the like that are surrounded by electrodes with transduced gaps on the order of less than 1 μm. All silicon MEMS resonators can be very small and rugged. They are intended for use in integrated circuits at higher frequencies [5.11].

5.2.2 Conventional Atomic Standards

Conventional atomic frequency standard designs are passive devices that are functionally illustrated in Fig. 5.6. The basic principle is to coherently excite transitions between two energy levels in the atom selected and detect that the transition has occurred. The frequency of the atomic transition is

$$\nu = \frac{E_2 - E_1}{h} , \tag{5.18}$$

where E_1 and E_2 are the energy levels of the atom and h is Planck's constant. An important characteristic of the selected transition is the line quality factor

$$Q_l = \frac{\nu}{\Delta\nu} , \tag{5.19}$$

where $\Delta\nu$ is the line width of the transition. The physics unit generating the precise clock signal incorporates a local oscillator to generate the atomic interrogation signal for the atomic transition and produce the stable output signal locked to the response to that signal. These devices are generally called passive devices because the atomic resonance portion does not actually oscillate but is interrogated with a signal that is modified by the atomic transition to the highly stable, or accurate, signal desired. The interrogation signal is produced by a local oscillator that is typically a quartz crystal oscillator frequency locked to the interrogation signal. The local oscillator may itself be an atomic clock used in a hybrid configuration. Selection or development of the local oscillator can be a significant item in itself.

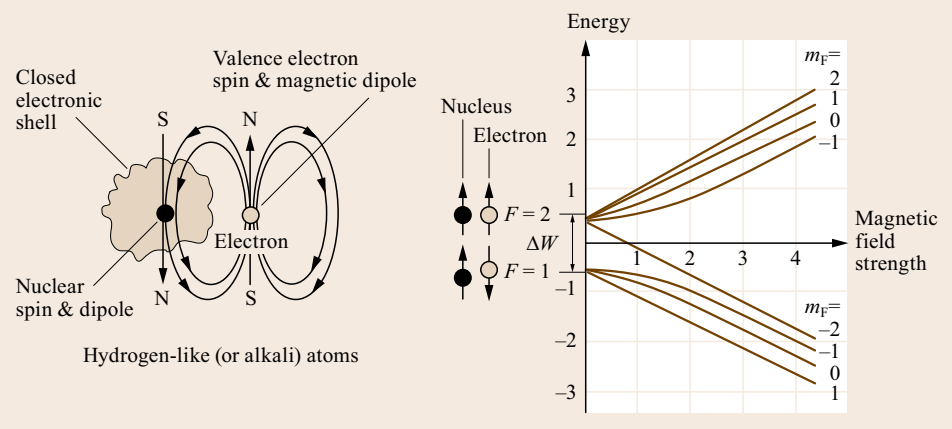

Fig. 5.7 Hyperfine structure of Rb87 with Zeeman splitting

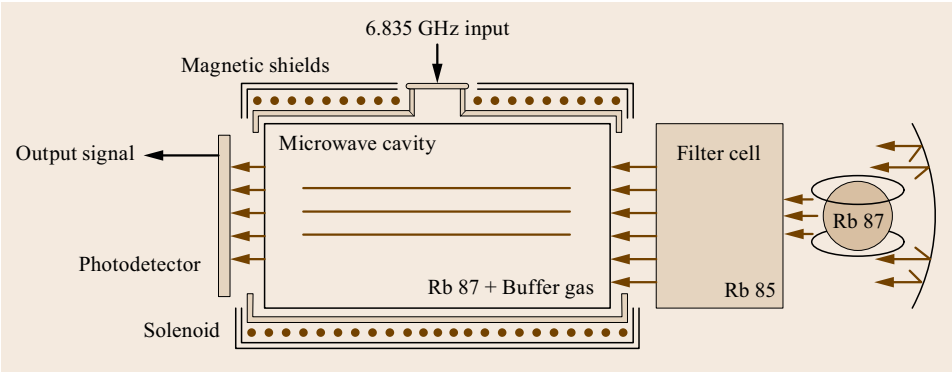

Fig. 5.8 Rubidium gas cell resonator

Rubidium Frequency Standards

Rubidium gas cell standards are the most commonly produced commercial atomic clocks. They are small, consuming relatively low power and are inexpensive in general. They are widely used in the telecommunications industry as frequency references for cellular telephone systems. They are also often found as internal frequency standards in laboratory instrumentation such as frequency counters, signal generators, and signal analyzers. Rubidium clocks were the first atomic clocks used in orbiting spacecraft and have become the primary clock technology used in the GPS satellites.

The rubidium transition used is the hyperfine ground state of Rb87. The hyperfine structure is illustrated in Fig. 5.7. F is the total angular momentum of the Rb87 atom and m_F is the quantized projection of F along a magnetic field. A transition between the two allowed energy states of F (which is reversing the spin of the valence electron) releases or absorbs an energy difference known as the hyperfine frequency of the ground state.

The atomic resonator shown Fig. 5.8 is an optically pumped device consisting of a series of glass cells containing small amounts of rubidium in gaseous suspension. The state of the rubidium atoms in the resonance cell are selected using light from an Rb87 lamp, which is filtered through a cell containing Rb85. The resonance cell also contains a buffer gas, typically nitrogen and argon or xenon, to hold the rubidium in suspension and to minimize interactions of the rubidium with the cell walls. The lamp is excited to a plasma with radio frequency (RF) energy creating the full set of Rb87 spectral lines. Only one of these lines is desired for interrogating the Rb87 atoms in the resonance cell. The Rb85 filter cell eliminates most of the unwanted spectral light, allowing a higher signal-to-noise ratio (SNR) at the photodetector. The Rb87 atoms in the resonance cell are at a controlled temperature and magnetic field to minimize environmental effects. The resonance cell is contained in a microwave cavity that creates a uniform RF field in the cell. The nominal frequency of the microwave cavity is about 6.834682611 GHz [5.12].

The overall design of a typical rubidium clock is shown in Fig. 5.9. When the 6.834682611 GHz signal is applied to the microwave cavity in the atomic resonator the level of the spectral light transmitted through the resonance cell is affected depending on how close the signal is to the inherent resonance of the Rb87 atoms.

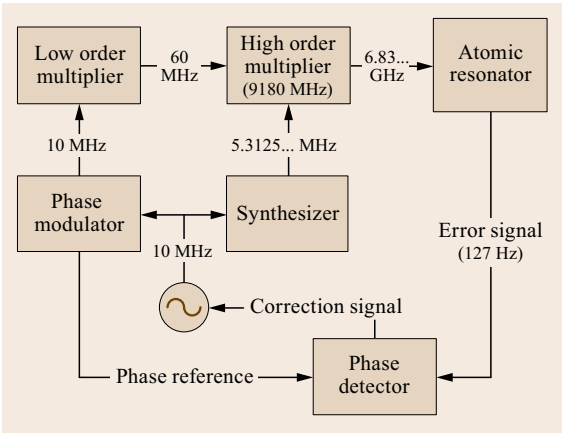

Fig. 5.9 Generic rubidium standard block diagram

An on-resonance signal will cause a decrease in the level of light transmitted through the resonance cell due to the absorption of the spectra. The microwave cavity signal is then modulated at about 127 Hz about the resonance so that the output of the photodetector provides an output signal proportional to the amount of light reaching it. This output signal is used as an error signal for the feedback loop, which adjusts the frequency of the crystal oscillator to minimize the error. The actual output signal is produced by the local oscillator.

This atomic interrogation technique is known as intensity optical pumping (IOP). Another optical technique employing lasers has been developed, known as coherent population trapping (CPT), which has been applied to Rb and Cs gas cell oscillators in smaller physical packages resulting in so-called miniature atomic clocks. This technique and its application to miniature clocks will be discussed later (Sect. 5.2.4).

Rubidium clocks based on the classic IOP design are considered to be secondary frequency standards because their inherent accuracy is significantly affected by the environment and the nature of the gas cell. These effects lead to environmental sensitivity and frequency drift. While rubidium clocks can be set on frequency very precisely, frequency drift rates exceeding 10^{-11}/month reduce absolute accuracy to some parts in 10^{-9}. Gas cell clocks of similar design can also be made using cesium or conceivably other alkali metals. However, using other atoms does not change the basic nature of the clock and does not make them primary standards for the reasons discussed in the next section.

Cesium Beam Frequency Standards

Cesium beam frequency standards are commercially available clocks and have been widely used for timekeeping and precise frequency generation, particularly in the telecommunications industry where they are used for clocking high-rate data streams. They are inherently much more accurate in frequency than rubidium clocks with accuracies as good as $5 \cdot 10^{-13}$. They also have an inherently very low frequency drift and reduced sensitivity to environmental effects, although the associated electronics in the units may be somewhat affected by environmental conditions, primarily temperature. Specially built cesium beam clocks with large long tubes designed for high accuracy have also been used as primary laboratory standards. Considering the small frequency shifts and the accuracy that can be maintained by a cesium beam frequency standard it is the most accurate device that is easily and commercially available.

The hyperfine frequency of the cesium atom in its ground state is the atomic transition used by these cesium standards. The ground state of Cs133 is the interaction between the hyperfine $F = 3$ and $F = 4$ energy levels. When a magnetic field is applied, the energy levels are divided into sublevels identified by their magnetic quantum number m_F. The frequency of the interaction $F = 3$, $m_F = 0$ to $F = 4$, $m_F = 0$ is the Cs hyperfine frequency, $\nu_{\mathrm{hf}} = 9.192631770\,\mathrm{MHz}$.

Because of the increased accuracy available from widely available commercial devices and the primary laboratory standards built for increased accuracy, the atomic second was adopted in 1967 as the basis of time in the Système International (SI) [5.13]. In continuity with previous timescales, the SI second has been defined as [5.14]:

> *[. . .] the duration of 9192631770 periods of the radiation corresponding to the transition between the two hyperfine levels of the ground state of the cesium 133 atom.*

Equivalently, the hyperfine frequency of the cesium atom's ground state amounts to exactly 9 192 631 770 Hz.

The commercial cesium beam tube, Fig. 5.10, is an atomic thermal beam device [5.15, 16]. The frequency ν of the hyperfine transition has a second-order dependence on the applied magnetic field (B in Teslas) of

$$\nu = \nu_{\mathrm{hf}} + 4.27 \cdot 10^{10}\,\mathrm{Hz} \cdot B^2 \,.$$

In operation, a cesium reservoir at one end of the sealed vacuum enclosure is heated to about 100 °C to produce a small stream of cesium atoms that is collimated into a beam. To limit the atoms in the beam to the useful energy levels, the desired energy states are magnetically selected and atoms in an undesired state are deflected out of the beam. The remaining atoms pass through a two-armed interrogation cavity known as a Ramsey cavity, where they are exposed twice to a microwave field. Here, the atoms change the ground state if the

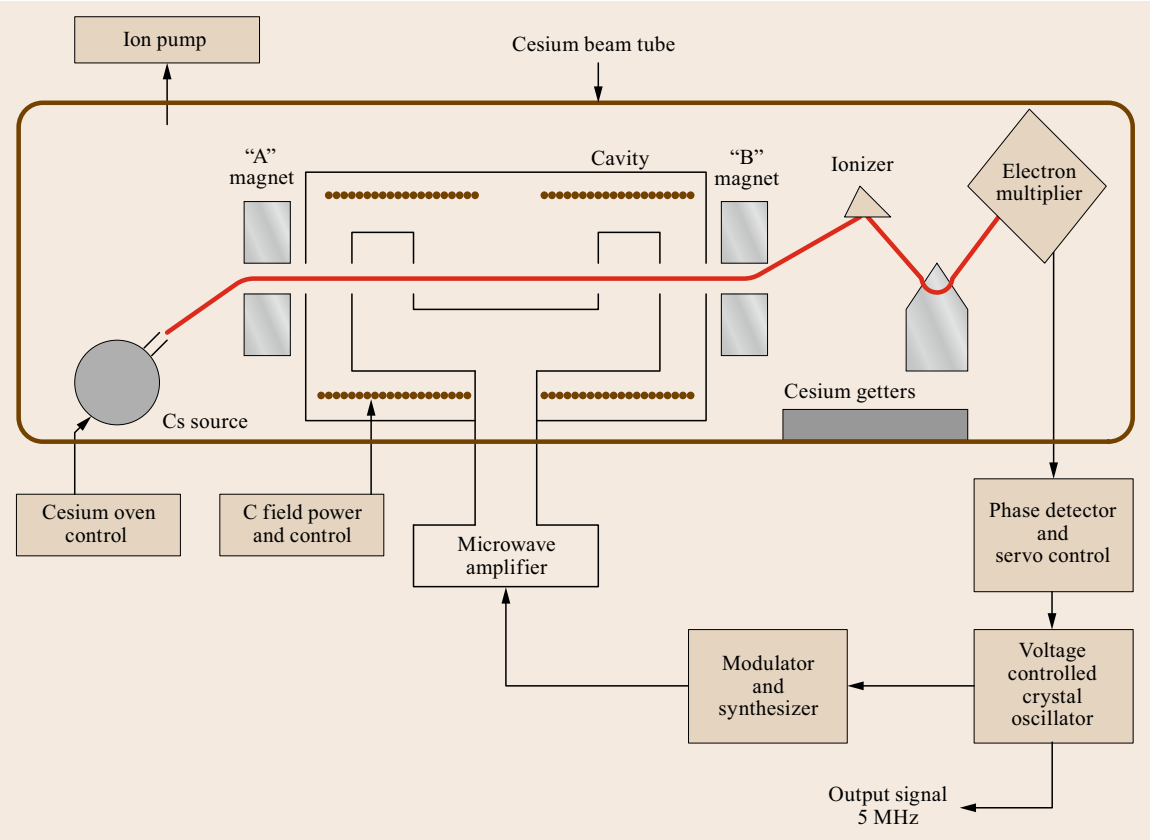

Fig. 5.10 Cesium beam tube diagram

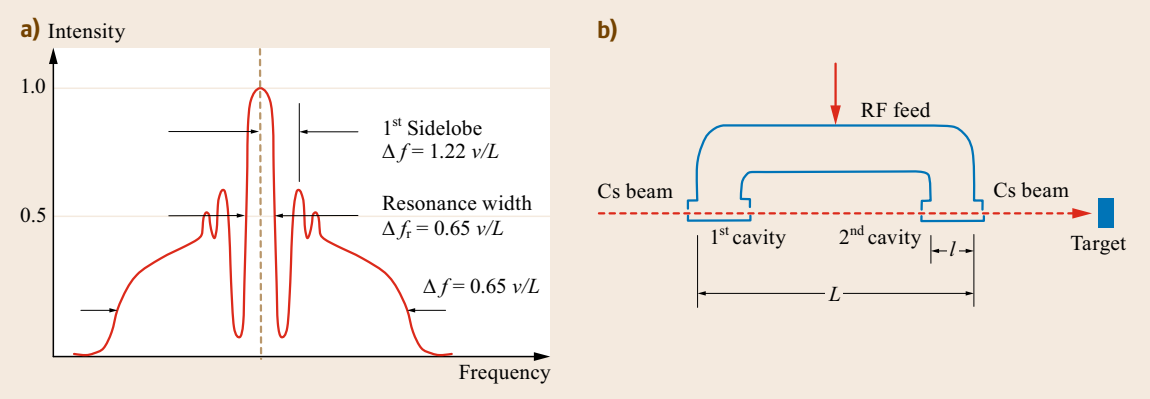

Fig. 5.11a,b Relation between the Ramsey pattern (**a**) and the dimensions L and l of the cavity (**b**). v denotes the velocity of atoms in the cesium beam

probing frequency matches the Cs hyperfine frequency. After leaving the cavity, the beam of cesium atoms passes through another magnetic state selector where atoms in the desired state are routed to a detector. Beam current from the electron multiplier is maximized when exactly the right microwave signal is present.

When varying the probing frequency around the nominal value, a resonance pattern with a line width inversely proportional to the cavity length is obtained. The structure of this *Ramsey* pattern is illustrated in Fig. 5.11. Since the slope of the change in frequency is zero at the peak, the direct measurement of the

resonance frequency from the Ramsey pattern is not suitable for a precise determination. Consequently, the microwave frequency is phase- or frequency-modulated so that an error signal can be generated by synchronous demodulation of the detector response. The frequency stability of the cesium beam standard then depends upon factors such as the modulation used in the microwave interrogation cavity and the frequency locking scheme. A generic block diagram of a cesium standard is illustrated in Fig. 5.12.

The frequency stability is approximately given by

$$\sigma_y(\tau) = \frac{K_{\mathrm{Cs}}}{Q_{\mathrm{l}} \cdot \left(\frac{S}{N}\right) \cdot \tau^{1/2}} , \qquad (5.20)$$

where $Q_{\mathrm{l}} = \nu/\Delta\nu$ is the line quality factor, S/N is the signal-to-noise ratio of the detected signal (the noise is mostly shot noise at the detector) and K_{Cs} is a factor dependent upon the modulation used but close to unity. In a typical, well-built laboratory primary standard a stability of $5 \cdot 10^{-12}\,\mathrm{s}^{1/2}/\tau^{1/2}$ over a range extending to 40 days has been measured.

Commercial cesium beam devices are widely available and in use today. However, the wide availability of GNSS timing receivers used to distribute precise time, their superior performance especially coupled with a rubidium clock and most notably their low cost has impacted the cesium frequency standard market. At this time, technology for primary laboratory and precision timekeeping devices has moved into cold atom technology applied to so-called fountain clocks, which will be discussed in Sect. 5.2.3.

Hydrogen Maser Frequency Standards

Hydrogen masers are the most stable frequency standards commercially available for use in laboratory and ground station environments. They have been developed for scientific, timekeeping and GNSS applications. There are two basic designs of hydrogen masers in use, the active maser where the maser cavity actually oscillates and produces a signal actively [5.17, 18], and the passive maser whose cavity is passively interrogated in a similar manner to the rubidium and cesium devices just discussed [5.19]. A third design of hydrogen maser known as the Q-enhanced maser [5.20] that can operate in either mode is briefly presented in Sect. 5.3.3.

The hydrogen maser operates at the ground state between the two hyperfine levels of atomic hydrogen ($F = 1$, $m_F = 0$ to $F = 0$, $m_F = 0$) at the ground state hyperfine frequency, ν_{hf}, of 1420.405752 MHz. The hyperfine energy levels of atomic hydrogen are shown in Fig. 5.13. The transition frequency depends on the magnetic field B (expressed in Teslas) and amounts to

$$\nu = \nu_{\mathrm{hf}} + 1399.08 \cdot 10^7\,\mathrm{Hz} \cdot B^2 . \qquad (5.21)$$

At room temperature the population of hydrogen atoms is nearly evenly distributed between four magnetic hyperfine levels designated by $F = 1$, $m_F = 1, 0, -1$ and $F = 0$, $m_F = 0$. These energy levels depend on the relative orientation of the magnetic dipoles associated with the proton and the electron when the atom is in a magnetic field. In the upper level, designated as $F = 1$, the angular momenta of the proton and electron are aligned and added. Their magnetic dipoles are also aligned. In this state the total angular momentum can orient itself with a magnetic field in three different directions and the $F = 1$ energy level splits into three components. The $F = 0$ energy level results from the alignment of protons and electrons that cancel their total angular momentum and their magnetic dipoles oppose each other.

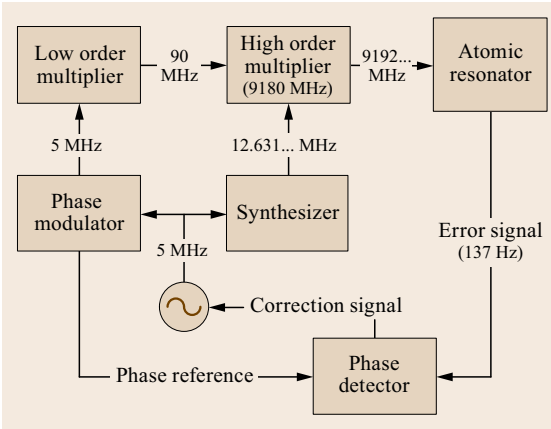

Fig. 5.12 Generic cesium beam standard block diagram

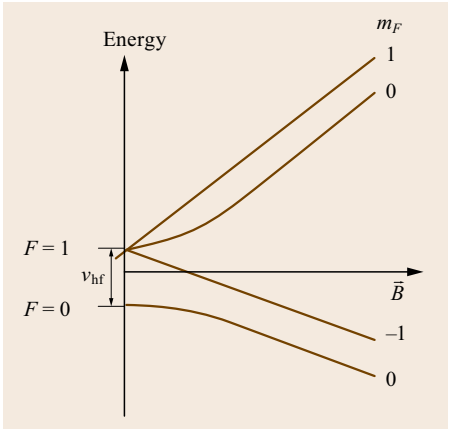

Fig. 5.13 Energy levels of atomic hydrogen

Figure 5.14 shows a schematic diagram of an active hydrogen maser. Molecular hydrogen at a pressure of about 0.1 Torr is dissociated into atomic hydrogen by an RF plasma discharge and collimated into a beam. Atoms in two of the upper magnetic hyperfine energy levels ($F = 1$, $m_F = 1$, and 0) are selected by passing through a highly inhomogeneous magnetic field generated by a multipole permanent magnet, which causes them to move toward the weak field near the axis of the magnet. These atoms are focused into a storage bulb located in a resonant microwave cavity tuned to the atomic hydrogen hyperfine frequency. The storage volume confines the atoms to a region where the oscillating magnetic field is in the same phase.

As the atoms proceed from the multipole magnet into the cavity bulb, the magnetic field they encounter changes from about 9 kGauss radially in the magnet to about one Gauss along the axis of the beam. In this drift region the atoms remain in the $F = 1$, $m_F = 1$, and 0 state and will be kept in these states along the drift region, if the magnetic field they encounter is reduced to the level of the field in the resonator without sudden interruption or change in direction.

A very important feature of an active hydrogen maser is the monomolecular Teflon surface coating in the storage bulb that enables its operation as an oscillator with a narrow resonance line width. This is achieved by storing the atoms without appreciable loss of phase coherence from collisions with the wall surfaces or each other.

The frequency of the $F = 1, m_F = 0$ to $F = 0, m_F = 0$ transition that powers the oscillator depends on the magnetic field. To avoid frequency shifts from changes in the magnetic field, hydrogen masers are operated at low magnetic fields. To maintain these low fields and provide a spatially uniform field, with variation at the micro-Gauss level throughout the bulb, magnetic shields are placed about the resonator to attenuate the outside magnetic field, and a solenoid is placed within the innermost shield to provide a uniform and controllable field.

Maser oscillation is sustained when the energy released by the incoming atoms resulting from stimulated emission of the microwave fields in the resonator exceeds the energy lost by the resonator. The energy loss includes the signal delivered to the receiver though a pickup loop in the microwave cavity that is mixed and compared to a signal from the local oscillator to produce the final output signal.

The fundamental stability limit for the maser is similar to other oscillators and is given as

$$\sigma_y(\tau) = \frac{1}{Q_l}\sqrt{\frac{kT}{2P\tau}}\,, \tag{5.22}$$

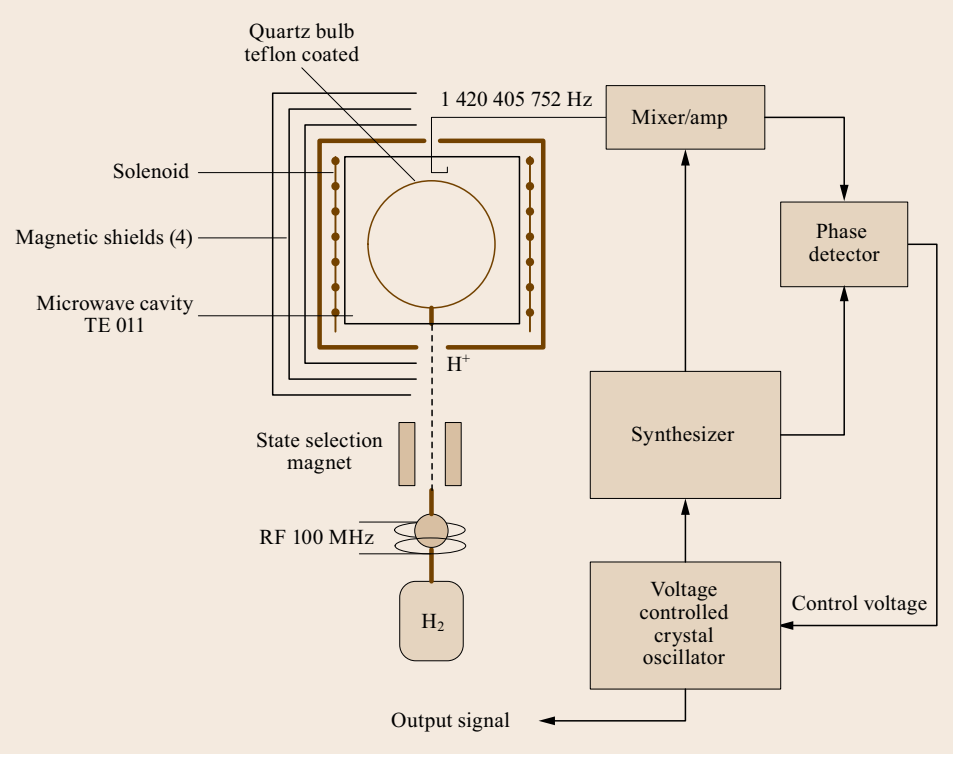

Fig. 5.14 Active hydrogen maser schematic

where Q_l is the line quality factor of the maser operating at a power level P, k is Boltzmann's constant, and T is the absolute temperature. This expression then implies high values for Q_l and power. However, high power also promotes increased interatomic collisions. Consequently masers typically operate with low power in which the signal-to-noise ratio of the receiver of the maser signal has a significant effect on the short-term stability (at $\tau < 100$ s).

A typical active maser uses a microwave cavity resonator operating in the TE_{011} mode. Without appreciable dielectric loading by the bulb, the resonator's dimensions are of a cylinder of 28 cm in diameter and height. These dimensions result in a storage bulb of two to three liters in size and a considerable large size to the overall maser with the levels of magnetic shielding and vacuum enclosure required. A reduced resonator size has been achieved by using dielectrically loaded cavities. In active mode, these smaller resonators tend to suffer larger thermal variations in resonance frequency due to the properties of the dielectric material used for loading the cavity and therefore require more thermal control than the unloaded resonators. However, used in the passive mode a considerable size reduction can be achieved. In those cases magnetron cavity designs have achieved a small resonator size with sufficient line Q_l for maser operation.

The smaller resonators using lumped capacitance loading to reduce dimensions are used in passive hydrogen maser and Q-enhanced hydrogen maser designs. Among others this type of resonator is used in the Russian Ch-176 hydrogen maser, some masers built by the Sigma-Tau Standards Corporation and in the small Q-enhanced spaceborne masers developed at the Hughes corporation for the US Naval Research Laboratory.

The use of a cavity loaded with dielectric material enables a smaller size of the cavity resonator, and is thus an important means for reducing the overall size of a hydrogen maser. However, the penalty is that the cavity Q_l will be lower and may be beneath the self-oscillating limit. Therefore the maser can be operated in the passive mode with two coupling loops whereby one injects a microwave signal into the cavity at the hyperfine frequency and another is used to detect the amplified signal. The energy from the injected signal causes stimulated emission of the atoms in the cavity. These smaller designs usually operate in the passive mode rather than the active mode just described.

A generic passive hydrogen maser design using a probe signal with two modulated frequencies is illustrated in Fig. 5.15. Here, the maser cavity is interrogated with a probe signal that is phase modulated at two different frequencies, f_1 that corresponds to the nom-

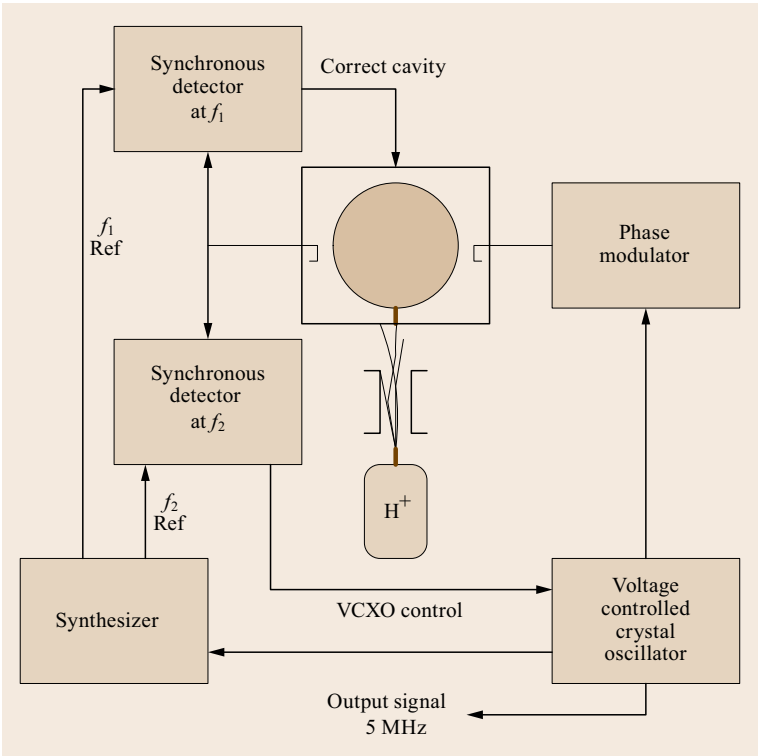

Fig. 5.15 Passive hydrogen maser schematic

inal half-width of the microwave cavity, and f_2 that corresponds to the nominal half-width of the hydrogen resonance. This phase-modulated probe signal is then coupled to the microwave cavity containing atomic hydrogen appropriately state selected. In the resulting spectrum the f_2 sidebands primarily interact with the narrow hydrogen line while the f_1 sidebands primarily interact with the broad cavity resonance. The signal transmitted from the cavity is amplitude modulated at frequencies f_1 and f_2. The size and sign of the amplitude modulation at f_2 relative to the impressed phase modulation is proportional to the frequency offset between the probe oscillator and the center of the hydrogen line. The microwave signal is envelope detected to recover the f_2 amplitude modulation, which is then processed in a synchronous or phase-sensitive detector reference to the f_2 phase modulation. The resulting error signal is used to correct the probe oscillator so that it is precisely centered on the hydrogen line.

Similarly, the f_1 phase modulation simultaneously probes the cavity resonance causing amplitude modulation of the transmitted microwave signal at f_1, which is proportional to the detuning of the microwave cavity from the center of the probe frequency. The error signal produced from the f_1 amplitude modulation in a synchronous detector is used to tune the microwave cavity to the probe frequency. This cavity servo technique then effectively stabilizes the mechanical dimensions of the cavity to reduce the effects of the environment, primarily temperature. Consequently, the maser cavity is environmentally stabilized and the interrogation frequency produced by the local voltage-controlled crystal oscillator (VCXO) is locked to the hydrogen resonance. The stability for this type of maser in the short term is not as good as the active maser due to the control servos however in the long term they approach similar performance.

5.2.3 Timescale Atomic Standards

Commercial cesium clocks are still the most prevalent standard for timekeeping in other than national timekeeping centers. Second is the active hydrogen maser that is in limited commercial availability. Both of these commercial devices are expensive with the hydrogen masers being about an order of magnitude more expensive than the cesium. The capability of GNSS timing receivers to disseminate time is increasing and many systems are using them to replace precise frequency and time standards as reference standards in timing applications (Chap. 41).

Within national timing centers, such as the National Institute of Standards and Technology (NIST) in the United States [5.21], the laser cooled cesium fountain has largely replaced the large thermal beam standards that were used as primary standards for determination of the SI second and contribution to the international atomic time scale. Unlike these other standards, cesium fountain clocks are not commercially available so that each center has built their own version. A number of different cesium fountain clocks are now in use throughout the world [5.22, 23] and in 2012 some 21 timing centers used cesium fountain clocks as their primary frequency standard. These primary standards serve as the metrologic reference and their performance is therefore determined by comparison and coordination with the Bureau International des Poids et Mesures (BIPM) [5.24].

The atomic fountain was first proposed and attempted by Jerrold Zacharias [5.23]. The original objective was to increase the interrogation time of a particular transition in the atoms beyond that possible in a thermal beam device by the use of gravity. If the atoms are launched upward through the same interaction region twice, the Ramsey fringes are produced with a resolution determined by the time between the two interactions. This significantly reduces the sources of errors since the same cavity would be used for both interactions. The design of fountain clocks has become practical through the use of laser cooling of trapped neutral alkali metals with atomic transitions in the microwave range, such as cesium and rubidium.

The development of the magneto-optical trap (MOT) provided the ideal method for trapping a number of neutral atoms and cooling them with laser radiation to within a few hundred micro-Kelvin of absolute zero [5.25]. The balls of cold atoms collected in the MOT could then be launched by the trapping lasers without significant heating and light shifts. This process is illustrated in Fig. 5.16. The atoms in a MOT are confined through the combination of laser field and magnetic field gradients, which can collect large samples of cold neutral atoms from background vapors or atomic beams. The trap geometry contains three intersecting orthogonal pairs of counter-propagating laser beams tuned just below a strong cycling transition in alkaline-earth and alkaline-earth-like atoms. The trapping region produces a three-dimensional optical molasses, so-called because the trap always provides a net force opposing the atom's propagation direction. The addition of a quadrupole magnetic field supplied by a pair of anti-Helmholtz coils forces the atoms toward the center of the trap. Millions of atoms can then be collected in a fraction of a second with an atomic temperature of approximately 1 mK.

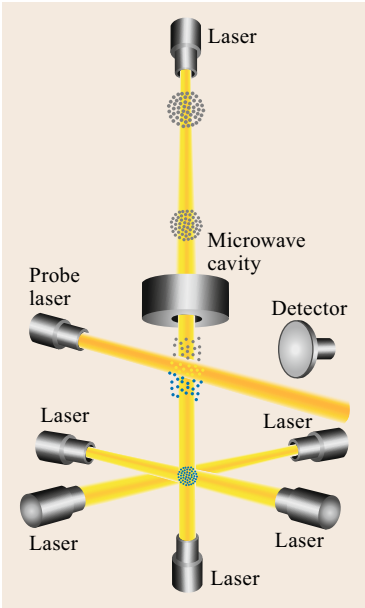

Fig. 5.16 Cesium fountain conceptual diagram (after [5.26]). Image courtesy of NIST

Atomic fountain clocks are based on this concept of laser cooling a collection of atoms to near absolute zero so that these atoms in a nearly-unperturbed neutral atomic state may be interrogated at the ground state hyperfine frequency [5.27]. Although the balls of atoms launched from the MOT contributing to the signal may have a comparatively small number of atoms, on the order of 10^3 to 10^6, the line quality factor Q_l is so large that a gain in frequency stability is obtained over the conventional thermal beam approach. It is shown that the frequency stability is given by the Allan deviation as

$$\sigma_y(\tau) = \frac{1}{\pi Q_l} \frac{\sigma(\Delta N)}{N} \sqrt{\frac{T}{\tau}}\,, \tag{5.23}$$

where $\sigma(\Delta N)$ is a variance measure of the fluctuations of the number of atoms from ball to ball, N is the average number of atoms in the balls and T is the cycle duration. In practice it is found that $\sigma_y(\tau)$ is about $3 \cdot 10^{-13}\,\mathrm{s}^{1/2}/\tau^{1/2}$, which is in agreement with the expression above.

Development of this technology has been facilitated by the availability of the appropriate lasers for the MOT and interrogation lasers. Diode lasers are the lasers of choice for use in fountain clocks and it is expected that there will be a significant synergy between cold atom development and space technology. The launch and operation of the Atomic Clock Ensemble in Space (ACES) experiment, which incorporates a cold atom cesium clock with a passive hydrogen maser, will demonstrate the potential of this type of laser-cooled standard in space [5.28].

5.2.4 Small Atomic Clock Technology

The capability of manufacturing very small or miniature atomic clocks was greatly enhanced by the development of a technique known as Coherent Population Trapping (CPT) [5.29]. It makes use of lasers for the optical pumping of clock transitions and been successfully employed with both Rb and Cs. Similar in concept to the classical Rb standard gas cell design, the spectral lamp is replaced by a diode laser at the required D_1 and D_2 wavelengths for Rb of 780 nm and 794 nm, or for Cs at 852 nm and 894 nm. Using diode lasers, the spectrum is much narrower than that produced by the spectral lamp, which improves the pumping efficiency. If the laser signal is modulated to produce two coherent signals at the wavelengths of the optical transitions corresponding to the levels $F = 2$ and $F = 1$ in the case of Rb a new phenomenon takes place. Coherent population optical pumping at the exact resonances with the optical transitions creates an interference resulting in the absence of the absorption of radiation.

The transition energy levels are illustrated in Fig. 5.17. The atoms are trapped in the ground state and find themselves in a nonabsorbing coherent superposition of the two hyperfine ground states. The atomic medium then becomes transparent at the exact resonance of the optical transition. The transmission of the cell increases at resonance and if the frequency of the laser signals is slowly swept, a resonance signal is observed at the photodetector. The shape of the signal is similar to the signals observed in the classical passive Rb standard described above.

In practice, the two laser signals may be obtained from a single laser modulated in frequency at a submultiple of the hyperfine frequency. The highly correlated sidebands created are used to provide the resonance signals. The technique may be used to implement a passive standard in either using the transmission (bright line) or the fluorescence (dark line).

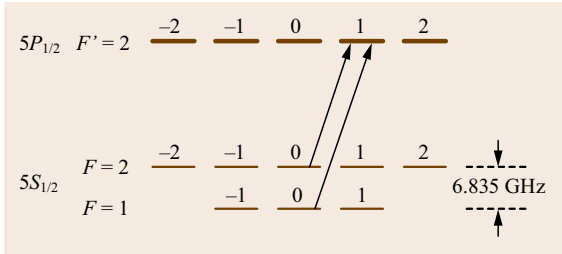

Fig. 5.17 The Rubidium CPT transition energy levels diagram

A microwave cavity is not needed since no microwave signals are required to excite transitions within the ground state. The design of a passive device is shown in Fig. 5.18.

The frequency stability of the CPT passive standard is expressed as approximately the same as that of the intensity optical pumped standard [5.29]

$$\sigma_y(\tau) = \frac{K}{4\,\nu_{\mathrm{hf}}\,q}\sqrt{\frac{e}{I_{\mathrm{bg}}\,\tau}}\,. \tag{5.24}$$

Here K is a constant depending upon the type of modulation used and is of the order of 0.2, e is the charge of the electron, I_{bg} is the background current created by the residual transmitted light reaching the photodetector, τ is the averaging time and q is a quality figure defined as the ratio of the contrast C to the line width. The contrast is defined as the CPT signal intensity divided by the background intensity.

The lack of requiring a microwave cavity facilitates the design of miniaturized atomic clocks down to a size limit determined by the laser and its corresponding performance limitations. The application of the CPT technique to cesium has resulted in a commercial product known as the chip scale atomic clock (CSAC) [5.30]. Preproduction units of the CSAC have demonstrated a stability of better than $3\cdot10^{-10}\,\mathrm{s}^{1/2}/\tau^{1/2}$ at timescales of at least 1–100 s [5.30]. When used in GNSS receivers, the improved stability helps to reduce phase noise, allows clock coasting during periods of reduced satellite visibility, and supports a faster time-to-first-fix (Chap. 13). Use of a stable atomic clock such as the CSAC inside a GNSS receiver has also been demonstrated as a technique for mitigating wideband radio frequency interference generated by GNSS jamming devices [5.31].

5.2.5 Developing Clock Technologies

Microwave standards are a mature technology and still have good potential for further significant improvements. For instance, a juggling rubidium fountain clock that launches multiple balls of atoms in rapid succession could greatly improve the SNR and result in short-term fractional frequency stability in the high 10^{-15}s at one second while still maintaining excellent long-term systematics well below 10^{-16}. This stability requires a local oscillator with better performance than an OCXO. The Time and Frequency Group at the Jet Propulsion Lab (JPL) in Pasadena has built a cryogenically cooled sapphire-loaded ruby oscillator that achieves $3\cdot10^{-15}$ performance from 1–1000 s, thus meeting the local oscillator requirements for an advanced fountain [5.32]. It is possible that further refinements to the fountain concept could bring that device into the low 10^{-15}s at a second.

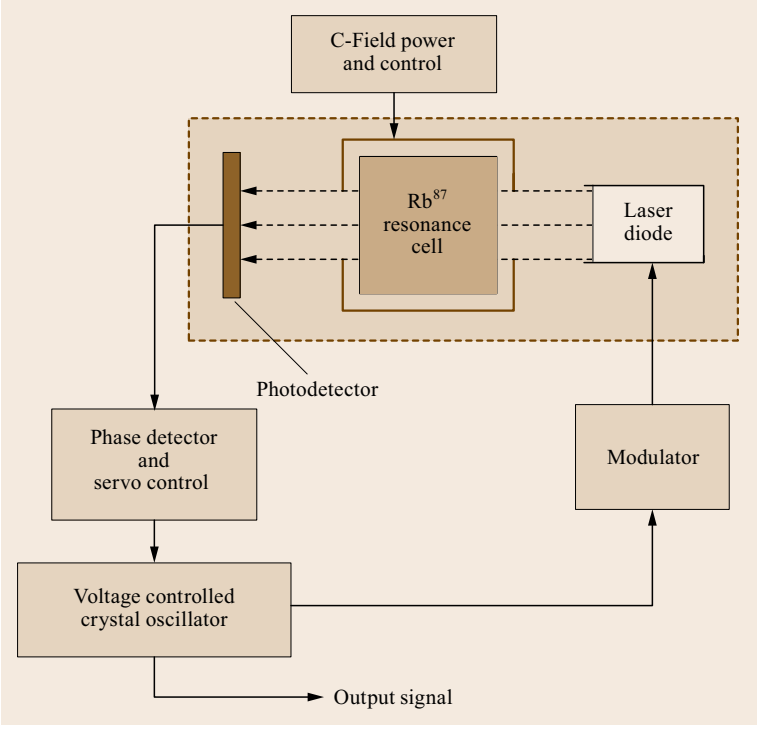

Fig. 5.18 Passive CPT rubidium clock

Laser-cooled microwave ion standards are expected to have an exceptional long-term systematic noise floor. It is likely that the main limitation will be magnetic field sensitivity, which is largely an engineering problem of providing good shielding while still maintaining good optical access. However, while the systematic floor is likely to be in the low 10^{-17}s, the short-term stability is probably limited to the low 10^{-13}s due to the low signal-to-noise ratio inherent in a device with only a few ions. As a result, a microwave laser-cooled ion trap device is unlikely to meet the stated goals.

Buffer-gas-cooled ion standards have already demonstrated a stability of $3 \cdot 10^{-14}$ at one second [5.33]. These devices have large signals (many ions) but only a moderate SNR due to large background signals. A factor of 3–10 improvement in SNR could be achieved with better detection schemes to reduce background. This almost certainly means using lasers instead of lamps as is the current practice. One of these ion standards coupled with an advanced local oscillator (such as the cryogenically-cooled oscillator already discussed) could get close to the short-term stability goal, but the systematic floor is unlikely to be below 10^{-16} (larger numbers of ions at higher temperatures means both exposure to higher RF fields and larger Doppler shifts). Nevertheless, this type of approach should not be dismissed too quickly, since this frequency stability still allows several picoseconds (ps) timing stability at one day. The buffer-gas-cooled ion standard with laser interrogation would require the fewest technological advances and would be the simplest to implement.

The next step in atomic clock evolution is to move from microwave clock frequencies to optical frequencies [5.34–36]. With frequencies measured in the 10^{15} Hz range instead of 10^{10} Hz, optical clocks have a potentially huge gain in line quality factor Q. Since short-term stability is inversely proportional to Q, it also improves. An ion trap clock based on an optical transition then combines very good short-term stability due to the high Q of the optical transition with an exceptionally low systematic noise floor. An optical clock is shown schematically in Fig. 5.19.

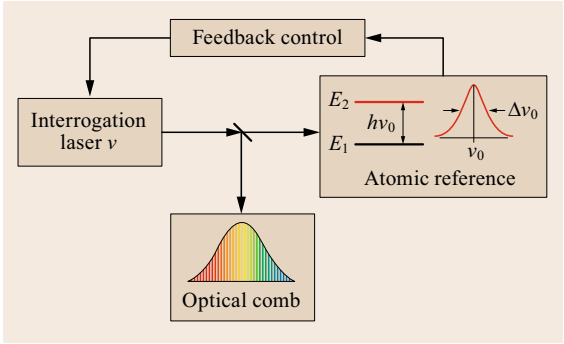

Fig. 5.19 Diagram of optical clock

The two technologies that are critical to optical clock progress are the optical comb and laser frequency stabilization. The optical comb (also known as the frequency comb) enables the coherent translation from optical frequencies to microwave frequencies where timing information is usually used, transferred and analyzed. This is a huge step for optical clocks, since previous chains linking optical to microwave frequencies required man-years of highly skilled work and large amounts of equipment to build and maintain. The second critical technology is laser frequency stabilization. To take full advantage of the optical line quality factor, the clock laser, which is now the local oscillator for this clock, must have a frequency uncertainty on the order of 1 Hz or less. This is difficult to achieve but offers great potential for future development of clock technology.

5.3 Space-Qualified Atomic Standards

The development of space-qualified atomic clocks has its origin in the navigation satellite concepts of the late 1960s and early 1970s. The Transit Doppler navigation system [5.37] first demonstrated the potential of worldwide high-accuracy navigation by satellite. These early navigation satellites were in a low altitude orbits, which provided sufficiently strong signals for users to calculate their position from the observed Doppler shift. The oscillator, or clock, had to be stable enough to permit a good frequency measurement over the period of time the satellites were in view. If the oscillator had a frequency change within that interval the frequency measurement would be in error creating a position error as well.

The advanced navigation satellite system designs, such as the Naval Research Laboratory (NRL) TIMATION (time navigation) concept and ultimately the Global Positioning System (GPS) were based on passive ranging to provide continuous accurate navigation to their users [5.38]. Development of space-qualified clocks for GPS was focused on predictable stability over time intervals of typically a day. From NRL work in the first phase of the GPS program (Block I) a space clock development program was formed to

develop space-qualified clocks for the NAVSTAR satellites [5.39]. To meet the system error requirements, projects in rubidium, cesium and hydrogen maser units were initiated. Improvements to the rubidium and cesium units used in the Block I demonstration satellite constellation were required to support the producibility, reliability and performance needs of the operational satellites (Block II/IIA) and alternative industrial sources for these units were required to be developed. The Block II/IIA GPS satellites contained two space cesium clocks and two rubidium clocks. Subsequent blocks of satellites, the replacement Block IIR and improved Block IIR-M contained three rubidium clocks and Block IIF contains two space rubidium and one space cesium clock. The next Block III satellites are to contain three rubidium clocks.

Developments of space-qualified atomic clocks have also been conducted for the Russian Federation GLONASS (global navigation satellite system), the European Galileo system, and the Chinese BeiDou navigation satellite system. Each GLONASS and GLONASS-M satellite hosts Russian three Cs-beam frequency standards [5.40], whereas the latest generation of GLONASS-K1 satellites is equipped with both cesium and rubidium clocks [5.41]. The Galileo satellites make use of passive hydrogen masers as their primary clocks in addition to conventional Rb gas cell frequency standards [5.42]. China, finally had a development project into space rubidium clocks since the initial deployment of BeiDou [5.43, 44] and is also investigating use of hydrogen masers for their global navigation systems [5.45].

Overviews of spaceborne atomic frequency standards and their use in the individual global and regional navigation satellite systems are given in [5.46] and [5.47]. The specific design aspects that distinguish spaceborne clocks from their terrestrial counterparts (such as environmental robustness and utmost reliability) are further discussed in [5.48].

5.3.1 Space Rubidium Atomic Clocks

The first atomic clocks in orbiting satellites were flown on board the Navigation Technology Satellite one (NTS-1) [5.49]. This satellite contained two quartz crystal clocks, developed under the TIMATION program, and two experimental rubidium clocks based on the FRK unit built by Efratom of Munich [5.50]. These rubidium clocks were commercial clocks modified as an experiment to survive the launch and thermal environment of space. Both rubidium units were encased in a large radiation shield to reduce the effects of radiation on the clock electronics. The performance of the NTS-1 rubidium clocks is shown in Fig. 5.20 in comparisons with the NTS-1 quartz oscillators and a cesium frequency standard flown later on the NTS-2 spacecraft. Despite a notable frequency drift at time exceeding several hours, these units provided the proof-of-concept necessary for use of rubidium clocks as primary units in the first NAVSTAR developmental satellites.

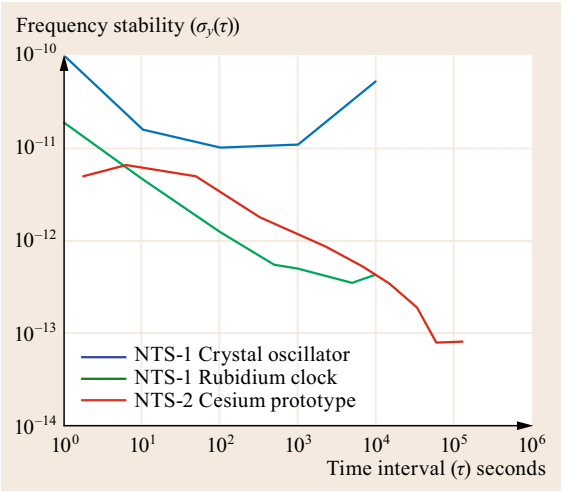

Fig. 5.20 Performance of NTS space clocks

The rubidium atomic clocks used in the early Block I GPS satellites were built by Rockwell International based on the FRK design of Efratom [5.51]. These units were a combination of an electronics design rebuilt for use in space by the Anaheim Division of Rockwell International and the physics portion built by Efratom. Fig. 5.21 shows the qualification unit of this design.

The early performance of the GPS units had a number of difficulties but they provided sufficient performance to support continued development. Nevertheless, the atomic clock of choice – and what was perceived to be the best clock for the final operational system (GPS Block II) – became the space-qualified cesium beam clock (Sect. 5.3.2), since it was a primary standard and did not exhibit the significant drift characteristic typical of rubidium. During the development of the GPS operational system in the 1980s alternative space-qualified atomic clocks were developed as part of the operational program of deployment [5.39]. The alternative source for space-qualified rubidium clocks was a design originally from EG&G, who became Perkin Elmer Optoelectronics and are currently known as Excelitas [5.52]. That company produced two prototype units that went on to become the atomic clock of choice for the GPS system during the Block IIR satellite deployment. Developments for GPS satellites focused on performance, improvements in the clock's state-of-health diagnostics, ground testability, and reduction of environmental sensitivities.

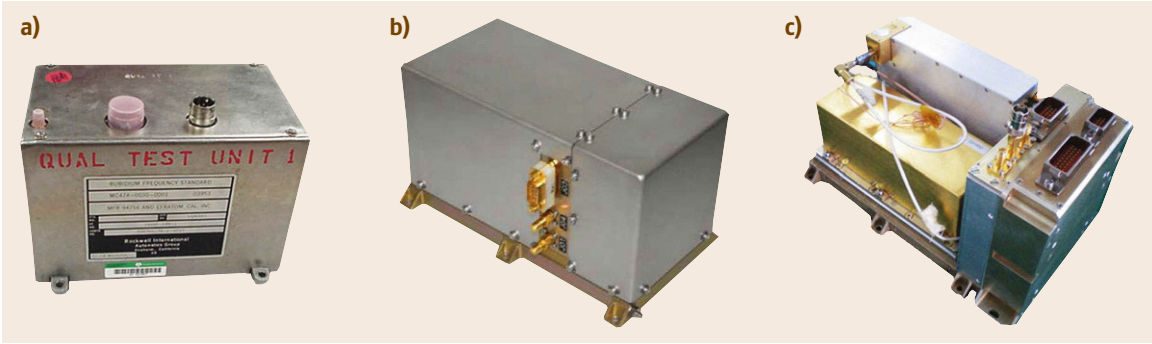

Fig. 5.21a–c Space-qualified rubidium clocks for GNSS Satellites: a qualification model for the early GPS satellites **(a)** (image courtesy of NRL), the RAFS developed by TEMEX/Spectratime for Galileo **(b)** (image courtesy of Spectratime), and the inside view of a second generation BeiDou rubidium clock **(c)** (after [5.44])

The latest version of Excelitas rubidium frequency standards used on board the GPS Block IIF satellites [5.53] as well as the *Michibiki* satellite of the Japanese quasi-zenith satellite system (QZSS) offer roughly a factor-of-two improvement in noise level and offer a stability of about $\sigma_y(\tau) = 1 \cdot 10^{-12}\,\mathrm{s}^{1/2}/\tau^{1/2}$. This is mainly achieved through the use of a xenon buffer gas and an advanced filter for the rubidium spectral lines that increase the overall quality factor [5.54]. Both the Block IIR and Block IIF operational rubidium clocks have demonstrated outstanding inflight performance as discussed further in Sect. 5.3.6.

Even though several BERYL Rubidium clocks [5.55] where flown on GLONASS precursor satellites [5.46], the Russian navigation has focused on the exclusive use of cesium beam frequency standards for more than 30 years (Sect. 5.3.2). Only recently, rubidium clocks have been introduced as alternative atomic frequency standards in the GLONASS-K series [5.41]. However, no flight results have become available up to the end of 2015.

Rubidum atomic frequency standards (RAFS) for the European Galileo program were originally developed under Swiss management by Spectratime (formerly Temex Neuchatel Time) along with Astrium, Germany, who did the space-qualified electronics [5.56]. The clocks exhibit representative stabilities of $\sigma_y(\tau) = 2\text{–}4 \cdot 10^{-12}\,\mathrm{s}^{1/2}/\tau^{1/2}$ and were flight tested in the GIOVE-A and -B satellites [5.57] prior to their selection and incorporation into the operational Galileo satellites. A sample of the Galileo RAFS is shown in Fig. 5.21. Complementary to the Galileo program, a variant using a Swiss electronic package has also been developed for use as backup clocks within the Chinese BeiDou constellation [5.47, 56]. Furthermore, the Specatratime Rubidium clocks are employed as primary frequency standards for the Indian Regional Navigation Satellite System (IRNSS; now known as NavIc for Navigation with Indian Constellation).

Along with the buildup of their national navigation satellite systems, various types of space-qualified rubidium clocks have also been developed in China. These indigenous RAFS exhibit a reported stability of about $5 \cdot 10^{-12}\,\mathrm{s}^{1/2}/\tau^{1/2}$ and presently serve as primary onboard clocks for the regional BeiDou navigation system. A recent RAFS model developed by the Beijing Institute of Radio Metrology and Measurement is shown in Fig. 5.21.

5.3.2 Space-Qualified Cesium Beam Clocks

The first prototype cesium clocks evaluated in orbit for GNSS were contained in NTS-2, which was the precursor of the NAVSTAR Block I satellites [5.38, 39, 58]. Two prototype cesium units were flown in NTS-2 and provided the space qualification of the cesium tube necessary for continued development. The cesium tube qualified in NTS-2 developed by Frequency and Time Systems Inc. (FTS) is shown in Fig. 5.22 and was the same tube used in the operational Block II/IIA GPS satellites. Performance of the NTS-2 cesium units in orbit is also shown in Fig. 5.20.

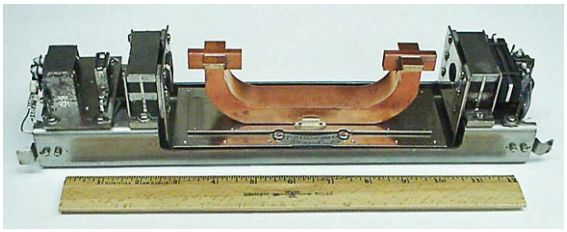

Fig. 5.22 Cesium beam tube without external shields and vacuum container showing the Ramsey cavity, the cesium reservoir on the right and detector assembly on the left. Image courtesy of NRL

During the next development step, engineering models of a refined design were built and tested. In cooperation with the US Defense Nuclear Agency, complete radiation testing was performed to determine the design parameters necessary for a radiation-hardened unit. The unit design and development with FTS continued through the preproduction model (PPM) stage. Six of these PPMs were built and provided to the prime satellite contractor Rockwell International (RI) for use in the early NAVSTAR satellites. The first PPM was launched in NAVSTAR 4 and the last would have been launched in NAVSTAR 7. This cesium design became the one employed in the Block II and IIA operational GPS satellites. These satellites had two cesium and two rubidium clocks in each satellite.

The next generation of cesium clocks for space were developed and deployed in the GPS Block IIF satellites [5.53]. These clocks employ a similar thermal cesium beam tube to that used in the earlier GPS satellites, but use digital electronics rather than the analog electronics used previously. The complete unit of the digital cesium beam frequency standard (DCFBS) for GPS Block IIF is shown in Fig. 5.23. It achieves a representative stability of $1 \cdot 10^{-12}\,\mathrm{s}^{1/2}/\tau^{1/2}$, and is mainly used as backup clock on those satellites. Its inflight performance is further described in Sect. 5.3.6.

Aside from GPS, cesium beam atomic clocks are also used extensively within the Russian GLONASS constellation, where they have served as the primary source of time and frequency information on most satellites launched so far. Satellites of the first generation GLONASS satellites were equipped with three GEM clocks [5.55] built by the Russian Institute of Radio Navigation and Time (RIRT), formerly Leningrad Scientific Research Radiotechnical Institute (LSRRI), in St. Petersburg. Only one clock is active at a time, while the others are kept in cold redundancy [5.40]. Even though the GLONASS clocks were operated in a sealed compartment at ambient pressure and temperature, their limited survivability posed a major constraint to the overall lifetime of those satellites [5.60].

Fig. 5.23 GPS Block IIF digital cesium beam frequency standard (DCFBS) from Symmetricom (after [5.59]). Reproduced with permission of MicroSemi

Satellites of the subsequent GLONASS-M series, which still makes up the majority of the current constellation, are equipped with MALAKHIT clocks that are likewise built by RIRT. Following [5.55, 61], the two clock types exhibit Allan deviations of about $1.5 \cdot 10^{-10}\,\mathrm{s}^{1/2}/\tau^{1/2}$ and $3 \cdot 10^{-11}\,\mathrm{s}^{1/2}/\tau^{1/2}$ at timescales of 100 s to one day. More recent developments have resulted in a performance improvement by a factor of 2–3 as well as a notably reduced mass of the GLONASS onboard frequency standards [5.62].

5.3.3 Space-Qualified Hydrogen Maser Clocks

The use of hydrogen masers for the ground stations and eventually in spacecraft was considered for GPS before the beginning of the program. Efforts at that time were based on adapting the active hydrogen maser design developed by the Smithsonian Astrophysical Observatory (SAO). SAO developed a series of active hydrogen masers for the Very Long Baseline Interferometry program that were capable of being operated in ground stations at remote sites. From that design, SAO built a space-qualified hydrogen maser for the National Aeronautics and Space Administration's (NASA) Gravity Probe One unit to investigate the gravitational relativistic effects on a precise clock. The probe was launched in the mid-1970s in a vertical ballistic trajectory to maximize the relativistic effects on the atomic clock [5.63]. The successful flight qualification and operation in the 2.5 h launch profile demonstrated the potential for operating such a clock in orbiting spacecraft. However, this particular active hydrogen maser design was rather large to consider incorporating into an orbiting satellite.

Reduction in the size of such a space clock was considered essential, so compact passive physics unit designs were investigated by NRL for GPS [5.64]. Various passive maser designs were investigated, both of the physics unit as well as electronics designs for cavity stabilization and interrogation. Several experimental units were built incorporating design alternatives for evaluation and the most successful approach was the Hughes Q-enhanced design incorporating a small magnetron cavity [5.65, 66]. This compact passive hydrogen maser design reduced the overall size of the device to roughly the size of a GPS space-qualified cesium clock.

Figure 5.24 shows the physics unit of the final version of the Hughes design.

The Galileo program also developed a small passive hydrogen maser (PHM) clock for operational satellites [5.67–69]. The development was jointly performed by Spectratime, Switzerland, and Galileo Avionica, Italy, who where in charge of the physics package and the electronics package, respectively. The maser cavities used in these devices are of similar design to that of the Q-enhanced maser design discussed above. They are a magnetron cavity design using a metal cavity machined to hold the hydrogen containment bulb with three arms that provide the capacitive loading on the cavity. The microwave cavity is thermally controlled to exhibit variations at the level of a few milli-Kelvin for baseplate temperature changes of about ±5 K. The Galileo PHM achieves a typical performance of $1 \cdot 10^{-12}\,\mathrm{s}^{1/2}/\tau^{1/2}$ over timescales of 1–10 000 s, which marks a notable performance increase over the Galileo RAFSs and makes it one of the best clocks ever used in navigation satellites. On the other hand, the mass of about 18 kg is notably larger than that of the rubidium clock. A flight-qualified space passive hydrogen maser ready for thermal vacuum testing is shown in Fig. 5.25. The PHMs for the Galileo program were flight tested on board the GIOVE-B technology demonstration satellite [5.57] and are now in routine use on board the operational Galileo satellites.

In parallel to the Galileo PHM developments, Observatoire de Neuchâtel and Spectratime pursued the development of a space-qualified, active hydrogen maser for use within the Atomic Clock Ensemble in Space (ACES [5.28]). The Space H-Maser (SHM) uses a sapphire loaded microwave cavity and achieves an Allan deviation down to $5 \cdot 10^{-15}$ at a timescale of 100 s [5.70, 71]. The larger mass (35 kg) and power consumption (77 W) of the active maser did not allow its consideration for the present Galileo system. Nevertheless, its use on ACES will provide further evidence for the potential of high-performance clocks in future navigation systems.

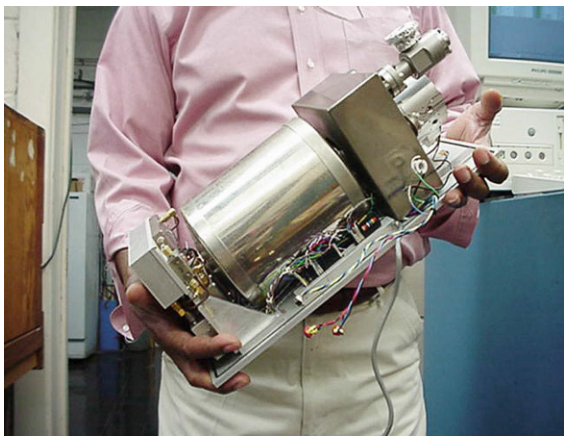

Fig. 5.24 Hughes Q-enhanced hydrogen maser physics unit. Image courtesy of NRL

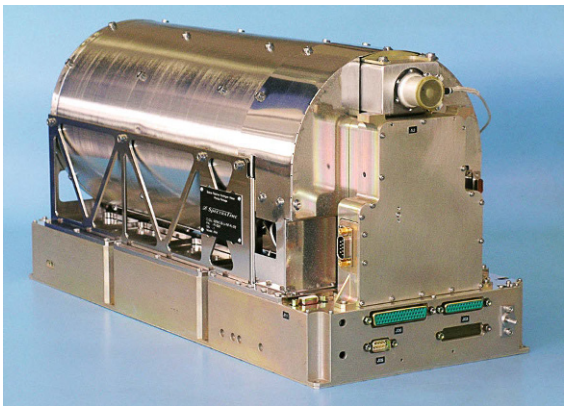

Fig. 5.25 Galileo space passive hydrogen maser. Image courtesy of Spectratime

5.3.4 Space Linear Ion Trap System (LITS)

The Jet Propulsion Laboratory Time and Frequency Group have developed a new technology standard known as the linear ion trap standard (LITS) [5.72]. Operational versions of these units are being deployed in the NASA Deep Space Network as replacements for the large active hydrogen masers currently in use. A spacecraft version of these units has been investigated and offers the potential of a very small size and power clock with potentially high stability. The physics package is small but since it is a passive device a high quality local oscillator is needed to gain the full potential of these devices. The potential performance gain using a modest performance local oscillator and the adaptability to digital implementation of the electronics could be a major step in spacecraft clocks [5.73]. NASA is currently developing a space-qualified version of this device for demonstration in a space environment [5.74].

5.3.5 Satellite Onboard Timing Subsystems

Aside from the atomic frequency standard, navigation satellite systems commonly employ some form of frequency distribution unit as part of their timing subsystem. Following [5.75], this unit may serve up to three purposes:

- Selection of one out of multiple clocks as the main source for the time and frequency generation

- Conversion of the native clock frequency to the base frequency for the navigation signal generation, and finally
- Performance of fine frequency adjustments to keep deviations of the onboard time from the GNSS time scale within specified limits.

In advanced timing system implementations, the above functions are combined with a monitor that compares the active clock against a reference to identify potential anomalies such as occasional bad points or outliers, phase jumps and frequency steps. All of these anomalous effects may happen singly, in combination, suddenly, or over a period of time. Serious situations related to satellite clock anomalies can be avoided by detection of these anomalies on board rather than through detection by tracking data on the ground. The clock's behavior can be better monitored on board in real time without additional noise or errors added by the communication link. However, multiple operating frequency standards on board are necessary to accomplish this result.

A well-known example of a timing subsystem taking care of the above functions is the Time Keeping System (TKS) of the GPS Block IIR satellites [5.76–78]. The TKS was originally designed to provide a common interface to different types of atomic clocks as well as determine the differences between the onboard atomic clocks and the output voltage-controlled crystal oscillator (VCXO). The system was configured to provide an interface for three atomic clocks, any one of which, when operating, was compared with a redundant VCXO by a phase comparator running at 600 MHz (Fig. 5.26). The VCXO produces the final signal but is adjusted or disciplined to the atomic clock's output. This intercomparison produces a measure of the onboard atomic clock's performance but it is ambiguous as to whether it occurs in the atomic clock or in the VCXO. Either one can affect the resultant comparison. At least three clocks would be necessary to be intercompared in order to produce an unambiguous determination of which clock produced the unacceptable performance [5.5].

In a similar fashion to GPS, the Galileo satellites utilize an onboard system called the clock monitoring and comparison unit (CMCU) [5.79–81] to monitor a standby clock with the clock driving the satellite transmitter (Fig. 5.27). Each Galileo satellite is equipped with two rubidium atomic frequency standards as well

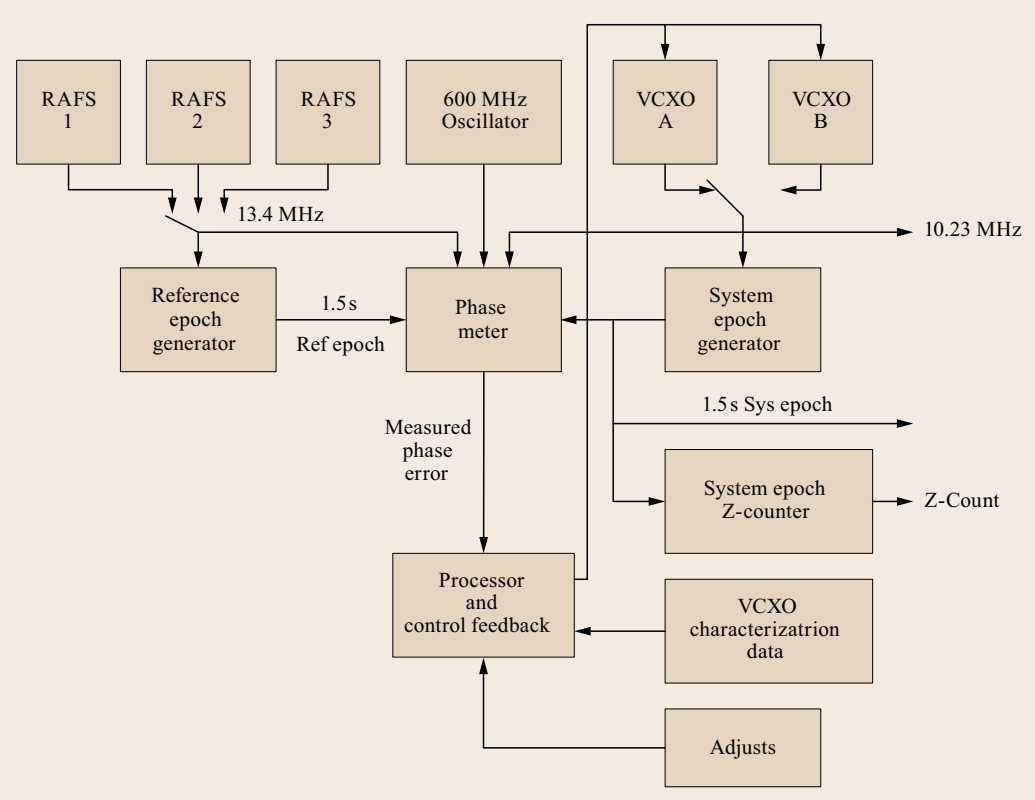

Fig. 5.26 Block diagram of Block IIR satellite Time Keeping System

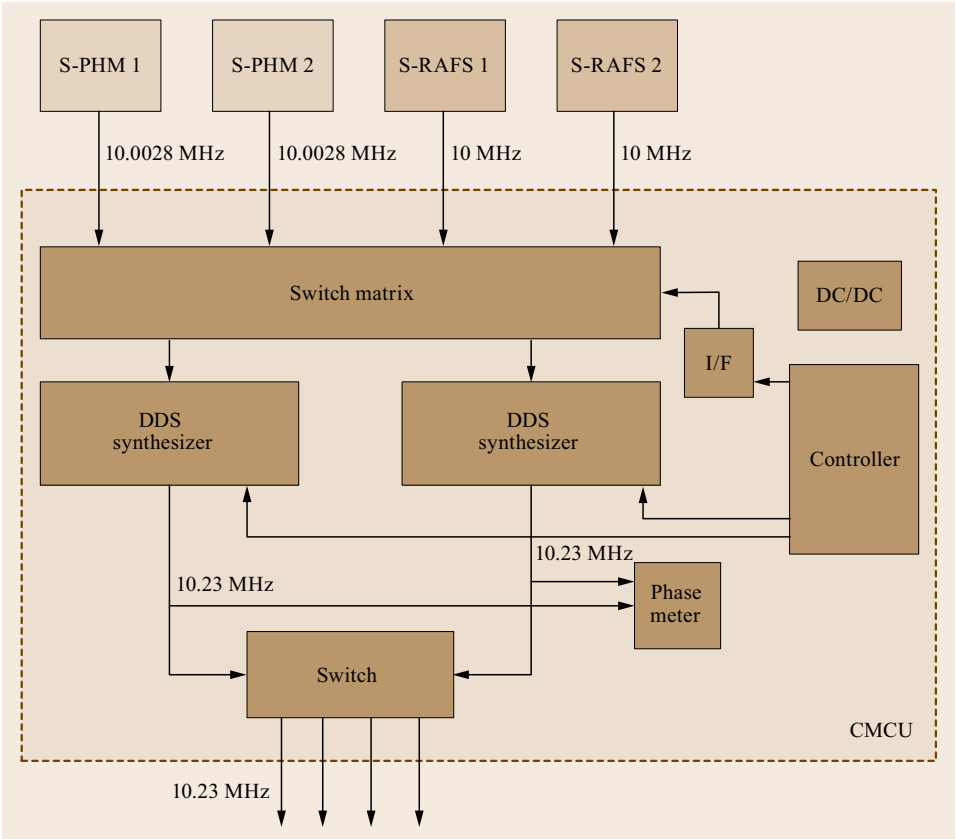

Fig. 5.27 Diagram of the Galileo clock monitoring and comparison unit

as two passive hydrogen masers. At any time, two of these four clocks are active while the other two serve as cold redundancy. Using a switching matrix, the signals of the two active clocks are connected to two synthesizers that shift the native clock frequency of 10 MHz for the RAFSs and 10.0028 MHz for the PHM by roughly 230 kHz to obtain the 10.23 MHz core frequency for the navigation signal. The synthesizers can be digitally controlled and enable adjustments of the output frequency in steps of less than 10^{-15} [5.81]. Even though only one synthesizer is selected to serve as master time reference, both outputs are continuously monitored through a phase meter. By continuously comparing the master clock with an operating standby clock, a switching transient and a loss of knowledge of the satellite time is avoided in case an immediate switch between both clocks needs to be made.

The onboard systems in use today are still mostly dependent upon the performance of a single clock to produce the desired performance. If clocks could be compared on board or with the signals from neighboring satellites provided satellite cross-links or signals from the other satellites could be made available, their outputs could be monitored to be less susceptible to interruption or anomaly but also to produce a somewhat more stable and accurate signal. This onboard comparison capability could provide an immediate detection of anomalies in the operational clock and if properly instrumented possibly even the navigation payload. The resulting status could be inserted into the navigation message for direct broadcast to the users in case of anomaly and to the ground monitoring stations, thereby providing a real-time alerting capability to the system. Data associated with the comparative indication could also be telemetered to the control segment for diagnostic and remedial actions. The current GNSSs do not perform a comparison between the onboard clocks sufficient for determination of clock anomalies. Instead they rely on ground monitoring for detection and correction of such anomalies. A more sophisticated measurement system would be necessary to support a technique for automatic detection and correction on board.

5.3.6 On-Orbit Performance of Space Atomic Clocks

The performance of atomic clocks on board the GNSS satellites is critical to the ultimate accuracy achievable

by the system. Today's satellite navigation systems operate primarily in a passive mode, where the satellites are tracked by a set of of monitoring stations. From these observations the system parameters, i. e., satellite ephemerides and clock correction values, are predicted ahead. The navigation information computed at the system master station is then uploaded into the satellites for transmission to the users over time [5.82]. Consequently, the ability to evaluate the clock performance in orbit and to accurately predict the system parameters is required. Effects contributing to the clock observations must be carefully modeled or eliminated, so that the observed and predicted satellite clock information will be as accurate as possible [5.83, 84].

Similar to GNSS-based positioning, the monitoring of GNSS satellite clocks makes use of pseudorange and carrier-phase observations. Both of these reflect measurements of the difference between the signal receive and transmit times relative to the local receiver and transmitter clocks. As indicated by the terminology, pseudoranges (and likewise the carrier-phase observations) do not represent a pure measurement of the distance ρ, but include contributions of the respective clock offsets relative to a common system timescale. As discussed in more detail in Chap. 19, the pseudorange p_i and carrier-phase observations φ_i on the i-th frequency ($i = 1, 2, \ldots$) can be modeled as

$$\begin{aligned} p_i &= \rho + c(dt_\mathrm{r} - dt^\mathrm{s}) + I_i + T + e_i \\ \varphi_i &= \rho + c(dt_\mathrm{r} - dt^\mathrm{s}) - I_i + T + A + \varepsilon_i \,, \end{aligned} \tag{5.25}$$

where c is the vacuum speed of light, ρ is the distance between the satellite antenna and the user receiver's antenna, dt_r is the clock synchronization offset of the user receiver's time, dt^s is the clock synchronization offset of the satellite's time at the time of transmission, I_i is the frequency dependent propagation delay due to the ionosphere and T is the delay due to the neutral atmosphere, mostly the troposphere. The measurements errors e_i and ε_i exhibit standard deviation at the decimeter and millimeter level, respectively, for pseudorange and carrier-phase observations. Even though carrier-phase measurements exhibit an extremely low noise, they also include an ambiguity A, which comprises both integer multiples of the wavelength and fractional-cycle phase biases. During uninterrupted tracking of a satellite signal the ambiguity is constant thus offering highly precise measurements of the range change and clock offset variations over time.

The various delays and errors associated with the observations are discussed in depth in Chap. 19. However, once the observations are corrected for instrumentation, equipment effects (antenna offsets and the like), propagation effects, geometric effects or delays, and satellite position relative to the receiving equipment are all compensated, the residual differences

$$\begin{aligned} cdt^\mathrm{s} - cdt_\mathrm{r} &= (\rho + I_i + T) - p_i + e_i \\ cdt^\mathrm{s} - cdt_\mathrm{r} - A &= (\rho - I_i + T) - \varphi_i + \varepsilon_i \end{aligned} \tag{5.26}$$

between the measurements and the modeled geometric range and propagation delays are basically a compari-

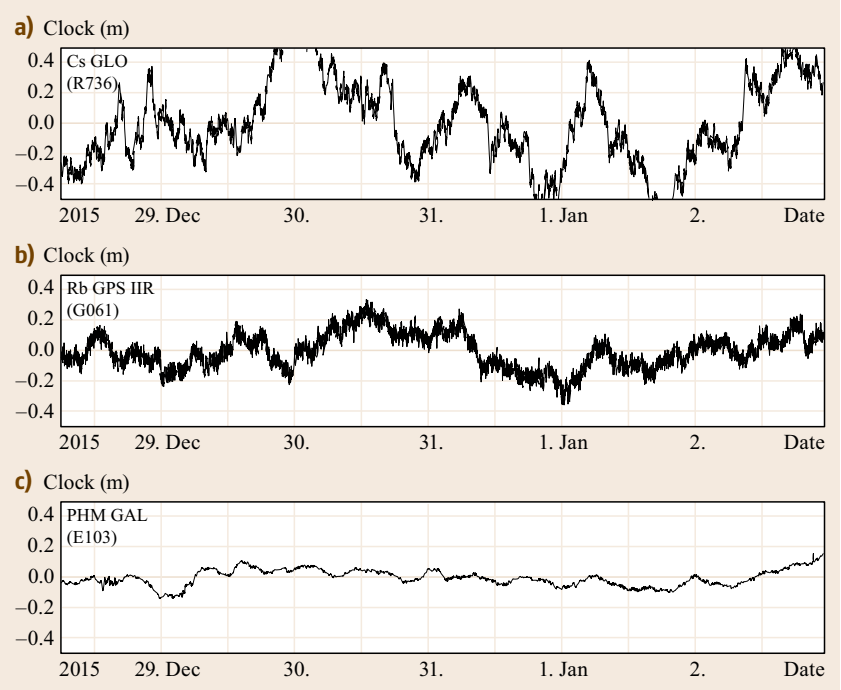

Fig. 5.28a–c Time series of observed clock offsets ($cdt^\mathrm{s} - cdt_\mathrm{r}$) for selected GNSS onboard frequency standards: GLONASS cesium clock **(a)**, GPS Block IIR rubidium clock **(b)**, and Galileo passive hydrogen maser **(c)**. All values are referred to a highly stable ground clock (active hydrogen maser) and have been detrended with a second-order polynomial. Values in brackets denote the space vehicle number of the respective GNSS satellites. Based on data from a multi-GNSS orbit and clock solution [5.85] of GeoForschungsZentrum (GFZ), Potsdam

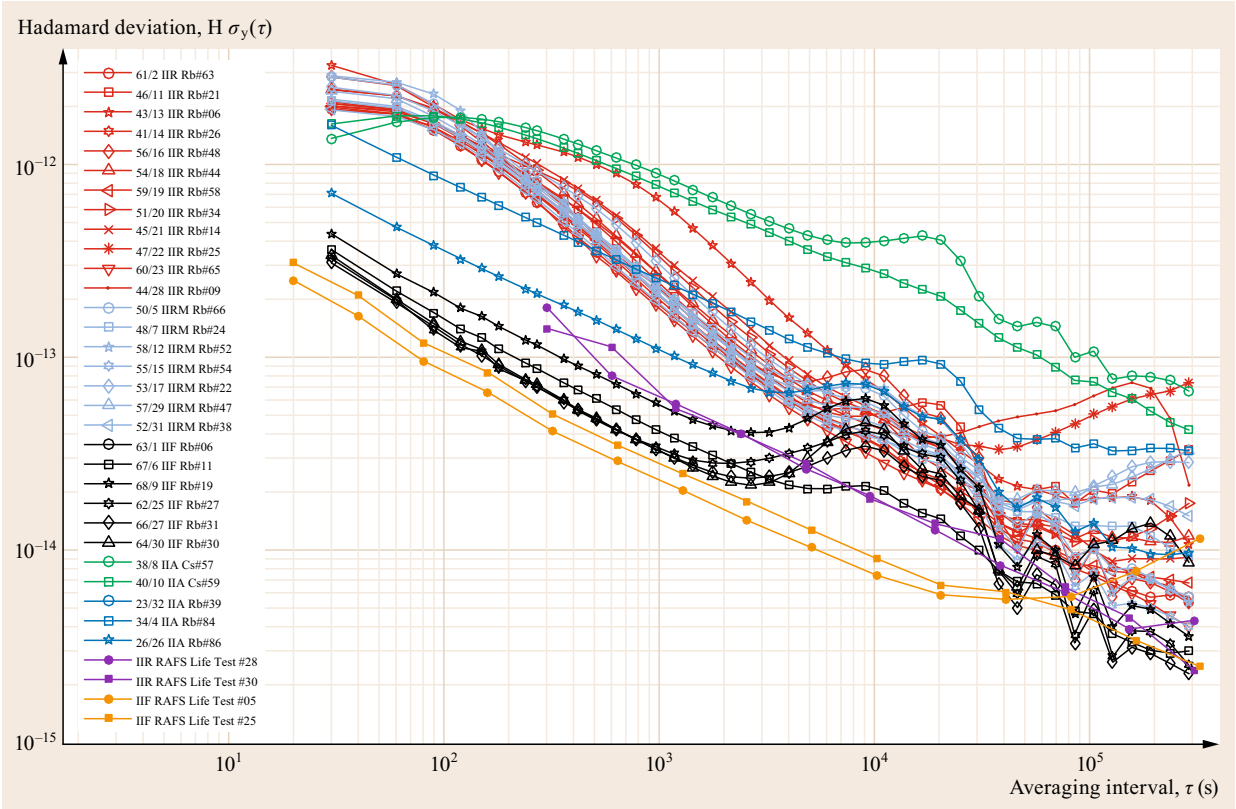

Fig. 5.29 On-orbit performance of GPS satellite clocks (Oct.–Dec. 2014). Individual satellites are identified by their space vehicle number (SVN)/pseudorandom noise (PRN) number. In addition the Block type and the active clock are indicated

son of two clock outputs just as they would be measured in a laboratory evaluation of two clocks. Examples of observed satellite clock offsets relative to a ground reference are shown in Fig. 5.28 for different GNSS satellites. The time series clearly reveal the different short- and long-term stability of individual types of atomic frequency standards.

Characterizing the satellite clocks' performance and predicting their performance ahead is dependent upon the ability to separate all other errors from the measurement so that only clock errors remain. This function is performed for the GNSSs by their respective tracking networks to support their operation. For GPS the network consists of the GPS Ground Segment tracking stations (Chap. 7) combined with additional stations operated by the National Geospatial-Intelligence Agency (NGA). This network supports the real-time operation of the GPS as well as providing the data for producing precise ephemerides for all the GPS satellites. In their support to the science community, the International GNSS Service (IGS; see Chap. 33) performs a similar function to provide highly accurate GNSS orbit products. The IGS data products have significantly reduced errors over that expected by normal navigation users. Details of the IGS product generation and the processes used to estimate satellite orbits, atmospheric parameters, site coordinates and Earth rotation parameters from a globally distributed network of monitoring stations are discussed in Chap. 34.

Clock offsets estimated from a global monitoring network as part of the precise orbit and clock determination process form a primary means for the inflight performance assessment of atomic frequency standards. In accord with the typical data rates and data arcs used in such adjustment processes, they mostly provide information on the clock stability at timescales of about 5 min to 1 day. For use at short timescales, the method is less suitable though, due to the high computational effort required for high-rate clock solutions. As an alternative, the *one-way carrier-phase* technique (OWCP) has been proposed in [5.86]. It makes use of carrier-phase observations from a single monitoring station connected to a highly stable reference clock (typically an active hydrogen maser). Based on (5.26) the difference of the onboard and ground clock is evaluated using a coarse orbit model such as broadcast ephemerides.

Subsequently, the resulting time series is detrended using a low-order polynomial to remove the impact of the carrier phase ambiguity and residual orbit errors as well as uncompensated atmospheric delays. Subject to a short data arc (up to a few hundred seconds) and the absence of large ionospheric variations, the method can even be applied with single-frequency observations rather than a more noisy dual-frequency combination.

Practical results and a comparison of the OWCP method with other clock estimates have, for example, been reported in [5.87–89]. The unique potential of this method to study the onboard clock stability at subsecond timescales has been demonstrated in [5.90] using GNSS receivers with data rates of 50 Hz and beyond. A special variant of the OWCP method has, furthermore, been studied in [5.91]. It makes use of the triangulation concept [5.92] for a statistical characterization of the clock noise, by processing data from three satellites simultaneously. This method does not require a highly stable ground clock, but relies on equal noise properties of all involved satellite clocks.

The space-qualified atomic clocks in the GPS operational satellites have stability requirements ranging from $2 \cdot 10^{-13}$ /day for cesium and $1 \cdot 10^{-14}$ /day for the rubidium on the later satellites. On-orbit performance has provided better than expected stabilities as demonstrated in Fig. 5.29. This figure provides the frequency stabilities of the GPS constellation clocks as measured by the Hadamard deviation calculated using the International GNSS Service (IGS) final clock products over the month of November 2013. For comparison with the on-orbit clock performance, Fig. 5.29 also shows the data from two Block IIF rubidium units under long-term test by the NRL. As the plots show, on-orbit performance of the Block IIF units is near that of the environmentally controlled ground units, at least over the short term.

Over longer averaging intervals the performance is degraded in comparison by apparent fixed period

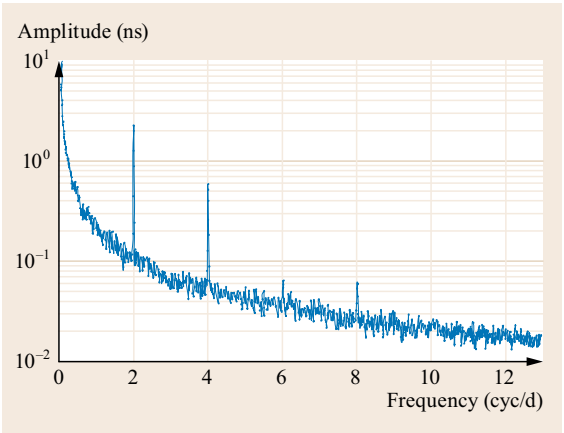

Fig. 5.30 Averaged amplitude spectrum of GPS constellation clocks (after [5.93])

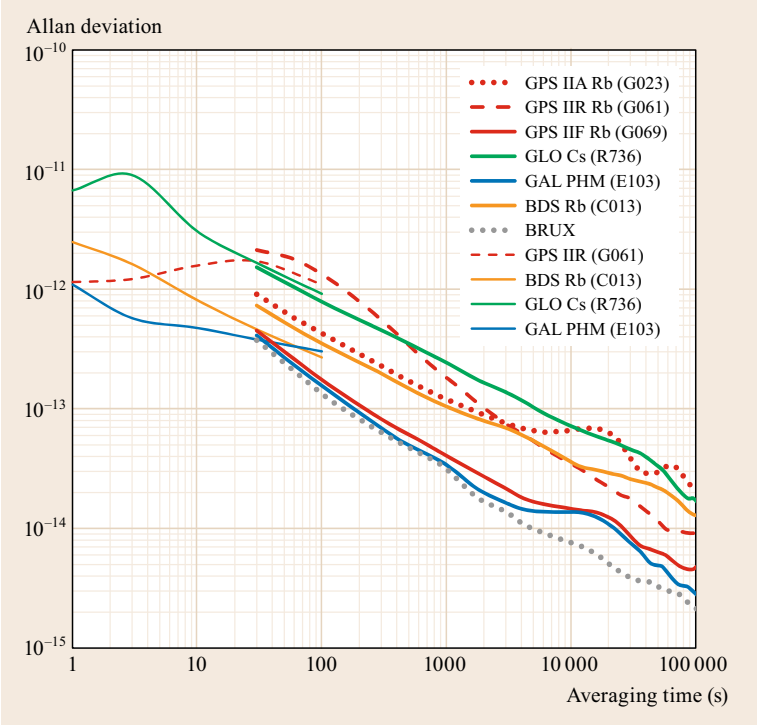

Fig. 5.31 Comparison of atomic clocks performances for current GNSS satellites. *Bold lines* provide Allan deviations for timescales of 30 s to 100 000 s based on data from the clock product of GeoForschungsZentrum (GFZ), Potsdam [5.85] for a one-week data arc in Jan. 2016. A *dotted gray* line provides the corresponding values for a hydrogen maser at the IGS GNSS station in Brussels. For comparison, *thin lines* show clock stability values over short timescales (1–100 s) as derived in [5.90] from a OWCP analysis

harmonic variations attributable to the satellite timing signal [5.93, 94]. The strongest of these harmonic variations occur nominally at 2.003 and 4.006 cycles per solar day with amplitudes of more than 2 ns for some GPS satellites. The Hadamard deviation statistic has a broad frequency response to pure harmonics so the harmonic variations are seen more distinctly using frequency domain techniques, as shown in Fig. 5.30. These data used individual satellite data spectra calculated by applying a standard periodogram with Blackman–Harris windowing to approximately 150 days of IGS final clock data for each satellite referenced to IGS time. The clock data for each satellite were detrended by fitting and removing a second-order polynomial prior to calculating its periodogram. The averaged spectrum was then obtained by averaging the individual satellite spectra at each Fourier frequency. Evidence is increasingly strong that the origin of the variations is likely to be thermal sensitivity, possibly of the associated electronics or of the units themselves.

A comparison of GPS atomic frequency standards with those of other navigation satellite systems in shown in Fig. 5.31 for timescales ranging from 1 s to more than a day. Stabilities for the various clock types differ by up to a factor of ten and are generally better for rubidium clock and hydrogen masers than for the currently employed cesium beam clocks. A superior performance can, in particular, be noted for the GPS IIF RAFS and the Galileo PHM, which exhibit stability values close to the observational limit over a wide range of timescales. While the Allan deviation follows the expected linear trend in the double-logarithmic representation for most clocks and satellites, bumps of varying amplitude can frequently be recognized at timescales near one half of the orbital period. These may be caused by thermal variations in the onboard equipment as discussed above, but can also be related to radial orbit errors induced by, for example, an incomplete modeling of solar radiation pressure forces [5.95]. On the other hand, ADEV bumps observed at timescales less than 1000 s for some types of GNSS satellites can often be attributed to the function of the respective timekeeping system [5.78].

5.4 Relativistic Effects on Clocks

The technologies of clocks, timekeeping, and GNSS have long advanced to a state where the precision of the measurements is on the order of nanoseconds and where such performance is necessary for satellite-based global navigation. To achieve this level of precision and accuracy, corrections imposed by relativity must be taken into account in addition to errors in the measurement systems, instrumental errors on board a satellite and atmospheric propagation delays. The development of GPS first brought a system into application, in which the principles of the special and general theories of relativity are not merely a matter of scientific interest, but have become an engineering necessity.

To understand the relationship between Coordinated Universal Time (UTC) reference timescale, its dependence on the International Atomic Time (TAI), their relation to the rotation of the Earth, as well as the time maintained and used by individual GNSSs, the relativistic relationship of timekeeping in and around the Earth is necessary [5.96]. In a relativistic formulation it is also necessary to have a clear understanding of the relationship of space-time reference systems in that framework. These relationships have been defined primarily by resolutions of the various international scientific organizations. The most important of these resolutions are:

1. International Astronomical Union (IAU) Resolution A4 (1991) defining the Geocentric Celestial Reference System (GCRS), the Barycentric Celestial Reference System (BCRS) and their time coordinates. IAU Resolution B1 (2000) further refines the BCRS definition.
2. International Union of Geodesy and Geophysics (IUGG) Resolution 2 (2007; see [5.96, Annex C]) defining the Geocentric Terrestrial Reference System (GTRS), along with the International Terrestrial Reference System (ITRS).

The nomenclature used here follows the IAU/IUGG framework in that the GCRS is known as the Earth-Centered Inertial (ECI) coordinate system, the GTRS (in practice, the ITRS) is known as the Earth-Centered Earth-Fixed (ECEF) coordinate system, and the BCRS is the barycentric coordinate system.

5.4.1 Relativistic Terms

GPS provided the initial theoretical model for relativistic synchronization and time comparison for GNSS development and operation as well as a laboratory for the validation of relativistic algorithms. However, the effects of relativity on precise orbiting vice orbit clocks

and the systems operating them should be understood in the context of global timekeeping. Relativistic formalism and relationships are based on observations and measurements between different frames of reference. Consequently an understanding of the different frames of reference and how they are realized in actual use is needed. This section will discuss a description of the relativistic effects on orbiting and Earth bound clocks and the implications for GNSS and other satellite-based time and position determination systems. This discussion is a prelude to understanding the issues of global timekeeping and GNSS timekeeping systems which are directly analogous.

GNSS internal timescales provide a basis for maintaining system internal synchronization and precision measurements between the elements of the system. The GNSS time is based on time maintained by sets of atomic clocks that are effectively generating versions of atomic time. They are linked to timekeeping centers so they can provide the most versatile and effective means of disseminating precise global time available.

The definition of some key relativistic terms and their meaning follows:

Proper time τ_p is the actual reading of a clock or the local time in the clock's own frame of reference.

Coordinate time t is the independent variable in the equations of motion of material bodies and in the equations of propagation of electromagnetic waves. It is a mathematical coordinate in the four-dimensional space-time of the coordinate system. For a given event, the coordinate time has the same value everywhere. Coordinate times are not measured; rather, they are computed from the proper times of clocks.

Space-time interval. The relation between coordinate time and proper time depends on the clock's position and state of motion in its gravitational environment and is derived by integration of the space-time interval. In the comparison of the proper times of two clocks, the coordinate time is ultimately eliminated. Thus the relativistic transfer of time between clocks is independent of the coordinate system. The coordinate system may be chosen arbitrarily on the basis of convenience.

In general, the space-time interval ds is described by

$$\begin{aligned} ds^2 &= g_{\mu\nu} dx^\mu dx^\nu \\ &= g_{00}c^2dt^2 + 2g_{0j}c\,dt\,dx^j + g_{ij}dx^i dx^j \,, \end{aligned} \tag{5.27}$$

where $g_{\mu\nu}$ are the components of the metric. In the notation used here a Greek index assumes the range 0, 1, 2, 3 and a Latin index assumes the range 1, 2, 3. A repeated index implies summation on that index. The metric depends upon the gravitational potentials, angular velocity and linear acceleration of the reference frame. Upon a transformation of the coordinates, the space-time interval remains invariant. Therefore the metric $g_{\mu\nu}$ transforms as a second-order covariant tensor.

The general expression for the relationship between proper time τ_p and the coordinates of the chosen coordinate system, comprising the coordinate time $x^0 \equiv ct$ and the spatial coordinates x^i, is given by

$$\begin{aligned} ds^2 &= g_{00}c^2dt^2 + 2g_{0j}c\,dt\,dx^j + g_{ij}dx^i dx^j \\ &= -c^2 d\tau_p^2 \,. \end{aligned} \tag{5.28}$$

Therefore $dt = d\tau_p$ for a clock at rest in an inertial frame of reference, for which $dx^i = 0$ and $-g_{00} = 1$, $g_{0j} = 0$, and $g_{ij} = \delta_{ij}$. The elapsed coordinate time corresponding to the measured proper time as registered by a clock along a path between points A and B is

$$\begin{aligned} \Delta t = \pm \int_A^B \frac{1}{\sqrt{-g_{00}}} \sqrt{1 + \frac{1}{c^2}\left(g_{ij} + \frac{g_{0i}g_{0j}}{-g_{00}}\right)\frac{dx^i}{d\tau_p}\frac{dx^j}{d\tau_p}}\,\mathrm{d}\tau_p \\ + \frac{1}{c}\int_A^B \frac{g_{0j}}{-g_{00}}\frac{dx^j}{d\tau_p}\mathrm{d}\tau_p \,. \end{aligned} \tag{5.29}$$

For an electromagnetic signal, the space-time interval is

$$ds^2 = g_{00}c^2dt^2 + 2g_{0j}c\,dt\,dx^j + g_{ij}dx^i dx^j = 0 \,. \tag{5.30}$$

The speed of light is c in every inertial frame of reference. The elapsed coordinate time of propagation along a path between points A and B is

$$\begin{aligned} \Delta t = \pm \int_A^B \frac{1}{\sqrt{-g_{00}}} \sqrt{1 + \frac{1}{c^2}\left(g_{ij} + \frac{g_{0i}g_{0j}}{-g_{00}}\right) dx^i dx^j} \\ + \frac{1}{c}\int_A^B \frac{g_{0j}}{-g_{00}}\mathrm{d}x^j \,, \end{aligned} \tag{5.31}$$

where the expression in parenthesis

$$\gamma_{ij} \equiv g_{ij} + \frac{g_{0i}g_{0j}}{-g_{00}}$$

represents the metric of three-dimensional space and

$$d\rho = \sqrt{\gamma_{ij}dx^i dx^j}$$

represents the increment of three-dimensional distance.

5.4.2 Coordinate Timescales

For practical purposes, different types of coordinate times are distinguished:

Geocentric Coordinate Time (TCG) is the coordinate time in a coordinate system with origin at the Earth's center (ECI or ECEF).

Terrestrial Time (TT) is the coordinate time that is rescaled from TCG so that it has approximately the same rate as the proper time of a clock at rest on the geoid. The geoid is the surface of constant gravity potential, which is closely approximated by mean sea level. The relationship between TCG and TT is defined such that

$$\frac{d(\mathrm{TT})}{d(\mathrm{TCG})} \equiv 1 - L_\mathrm{G} \,,$$

where

$$L_\mathrm{G} \equiv 6.969290134 \cdot 10^{-10} \approx 60.2\,\mu\mathrm{s/d}$$

as discussed below. The value of L_G is a defined constant. Consequently,

$$\begin{aligned}\mathrm{TCG} - \mathrm{TT} &= L_\mathrm{G}(\mathrm{TCG} - \mathrm{TCG}_0) \\ &= \frac{L_\mathrm{G}}{1 - L_\mathrm{G}}(\mathrm{TT} - \mathrm{TT}_0) \,,\end{aligned}$$

where TCG_0 and TT_0 correspond to JD 2 443 144.5 TAI (1977 Jan. 1, 0 h). The practical realization of TT is

$$\mathrm{TT} = \mathrm{TAI} + 32.184\,\mathrm{s} \,. \tag{5.32}$$

Barycentric Coordinate Time (TCB) is the coordinate time in a coordinate system with origin at the solar system barycenter. The coordinate time difference between TCB and TCG is a transformation that depends on both time and position. This timescale is important to be used when the satellite is outside Earth orbit and the influence of the Solar System needs to be taken into account.

5.4.3 Geocentric Coordinate Systems

The following section will discuss the transformation between the proper time of an ideal clock (one that exactly realizes the SI second) and coordinate time in a geocentric coordinate systems.

Earth-Centered Inertial Coordinate System

The coordinate time associated with an Earth-centered inertial (ECI) coordinate system is TCG. Through terms of order $1/c^2$, the components of the metric tensor in this coordinate system are

$$\begin{aligned} -g_{00} &= 1 - \frac{2U}{c^2} \,, \\ g_{0j} &= 0 \,, \\ g_{ij} &= \left(1 + \frac{2U}{c^2}\right)\delta_{ij} \,, \end{aligned} \tag{5.33}$$

where U is the gravitational potential. The elapsed TCG in the ECI coordinate system corresponding to the elapsed proper time as registered by a clock moving along a path between points A and B with velocity v is given by

$$\Delta t = \int_\mathrm{A}^\mathrm{B} \left(1 + \frac{1}{c^2}U + \frac{1}{2c^2}v^2\right) \mathrm{d}\tau_\mathrm{p} \,. \tag{5.34}$$

The Earth's potential U at radial distance r, geocentric latitude ϕ, and longitude λ may be expressed as an expansion in spherical harmonics

$$\begin{aligned} U(r,\phi,\lambda) &= \frac{\mathrm{GM}_\oplus}{r}\left[1 + \sum_{n=2}^{\infty}\sum_{m=0}^{n}\left(\frac{\mathrm{R}_\oplus}{r}\right)^n \right. \\ &\qquad \left. \times P_{nm}(\sin\phi)(C_{nm}\cos m\lambda + S_{nm}\sin m\lambda)\right] \end{aligned} \tag{5.35}$$

with coefficients C_{nm} and S_{nm}. Here, $\mathrm{GM}_\oplus$ is the gravitational coefficient of the Earth and $\mathrm{R}_\oplus$ its equatorial radius. Furthermore, the factors P_{nm} denote the associated Legendre functions of degree n and order m.

For practical applications it is sufficient to include only the Earth oblateness correction and approximate the gravitational potential as

$$\begin{aligned} U &= \frac{\mathrm{GM}_\oplus}{r} \\ &\quad + J_2\frac{\mathrm{GM}_\oplus}{r}\left(\frac{\mathrm{R}_\oplus}{r}\right)^2 \frac{1}{2}\left(1 - 3\sin^2\phi\right) \,, \end{aligned} \tag{5.36}$$

where $J_2 = -C_{2,0} \approx 1.08 \cdot 10^{-3}$ is the leading zonal gravity coefficient.

Even for a clock at rest on the surface of the rotating Earth, it is necessary to account for its velocity $\boldsymbol{v} = \boldsymbol{\omega} \times \boldsymbol{r}$ in the ECI coordinate system, where $\boldsymbol{\omega}$ is the angular velocity of the Earth and $\boldsymbol{r}$ is the position of the clock. Thus TCG elapsed as the clock records proper time $\Delta\tau_\mathrm{p}$

is

$$\Delta t = \int_A^B \left(1 + \frac{1}{c^2}U + \frac{1}{2c^2}||\boldsymbol{\omega}\times\boldsymbol{r}||^2\right) = \int_A^B \left(1 + \frac{1}{c^2}W\right) \mathrm{d}\tau_\mathrm{p}\,, \tag{5.37}$$

where

$$W = U + \frac{1}{2}||\boldsymbol{\omega}\times\boldsymbol{r}||^2 = U + \frac{1}{2}\omega^2 r^2 \cos^2\phi \tag{5.38}$$

is the gravity potential.

As the gravity potential W_0 over the surface of the geoid is constant, it may be evaluated on the equator and is approximately given by

$$W_0 \approx \frac{GM_\oplus}{R_\oplus}\left(1 + \frac{1}{2}J_2\right) + \frac{1}{2}\omega^2 {R_\oplus}^2\,. \tag{5.39}$$

The current best estimate of W_0 is $6.2636856\cdot 10^7\,\mathrm{m}^2/\mathrm{s}^2$.

According to (5.37), the TCG in the ECI coordinate system that corresponds to the proper time $\Delta\tau_{\mathrm{p}0}$ measured by a clock at rest on the geoid is

$$\Delta t \equiv \mathrm{TCG} = \left(1 + \frac{W_0}{c^2}\right)\Delta\tau_{\mathrm{p}0} \approx (1 + L_\mathrm{G})\Delta\tau_{\mathrm{p}0}\,, \tag{5.40}$$

where $L_\mathrm{G} \equiv 6.969290134\cdot 10^{-10}$. By convention, the value of L_G is a defined constant. It represents the best available value of W_0/c^2 at the time of its definition in 2000 [5.96].

TT is obtained by rescaling TCG by the factor $1 - L_\mathrm{G}$. Thus

$$\Delta t' \equiv \mathrm{TT} = (1 - L_\mathrm{G})\mathrm{TCG}\,. \tag{5.41}$$

It follows that

$$\mathrm{TT} = (1 - L_\mathrm{G})(1 + L_\mathrm{G})\Delta\tau_{\mathrm{p}0} \approx \Delta\tau_{\mathrm{p}0}$$

to within a few parts in 10^{18}.

For a clock on an Earth-orbiting satellite, the orbit may be regarded as Keplerian (unperturbed) in the first approximation (Chap. 3). The potential at distance r from the Earth's center is approximately $U = GM_\oplus/r$. Therefore the increment of TCG is

$$\Delta t = \int_A^B \left(1 + \frac{1}{c^2}\frac{GM_\oplus}{r} + \frac{1}{2c^2}v^2\right)\mathrm{d}\tau_\mathrm{p}. \tag{5.42}$$

The variation of the satellite velocity v with distance r is determined from the conservation of the specific energy

$$\varepsilon = \frac{1}{2}v^2 - U = \frac{1}{2}v^2 - \frac{GM_\oplus}{r}\,, \tag{5.43}$$

which amounts to

$$\varepsilon = -\frac{GM_\oplus}{2a} \tag{5.44}$$

for an orbit of semimajor axis a. Therefore, to this order of approximation, the elapsed coordinate time is

$$\Delta t = \int_A^B \left(1 - \frac{1}{c^2}\frac{GM_\oplus}{2a} + \frac{1}{c^2}\frac{2GM_\oplus}{r}\right)\mathrm{d}\tau_\mathrm{p} = \left(1 - \frac{1}{c^2}\frac{GM_\oplus}{2a}\right)\Delta\tau_\mathrm{p} + \frac{2GM_\oplus}{c^2}\int_{t_0}^{t}\frac{1}{r}\mathrm{d}t\,. \tag{5.45}$$

In the last integral $\mathrm{d}\tau_\mathrm{p}$ has been replaced by $\mathrm{d}t$ as this term is a relativistic correction of order $1/c^2$.

For a Keplerian orbit the radial distance is given by

$$r = a(1 - e\cos E)\,,$$

where e is the orbital eccentricity and E is the eccentric anomaly. The eccentric anomaly is determined from the mean anomaly by Kepler's equation

$$M \equiv n\Delta t = E - e\sin E\,,$$

where

$$n \equiv \frac{2\pi}{T} = \sqrt{\frac{GM_\oplus}{a^3}}$$

is the mean motion and T is the orbital period (Chap. 3). Therefore, the TCG elapsed as the clock records proper time $\Delta\tau_\mathrm{p}$ is approximately

$$\Delta t = \int_A^B \left(1 - \frac{1}{c^2}\frac{GM_\oplus}{2a} + \frac{1}{c^2}\frac{2GM_\oplus}{r}\right)\mathrm{d}\tau_\mathrm{p} = \left(1 + \frac{3}{2}\frac{1}{c^2}\frac{GM_\oplus}{a}\right)\Delta\tau_\mathrm{p} + \frac{2}{c^2}\sqrt{GM_\oplus a}\cdot e\sin E\,.$$

The second term is a periodic correction due to the orbital eccentricity that causes a residual variation in distance and velocity given by

$$\Delta t_{\mathrm{ecc}} = \frac{2}{c^2}\sqrt{GM_\oplus a}\cdot e\sin E = \frac{2}{c^2}(\boldsymbol{v}\cdot\boldsymbol{r})\,. \tag{5.46}$$

To compare the proper time of a clock on a satellite with the proper time of a clock at rest on the geoid, it is necessary to convert from TCG to TT. By (5.41) and (5.42), the result is (TT)

$$\begin{aligned}\Delta t' &= (1-L_{\mathrm{G}})\Delta t\\ &= \int_{\mathrm{A}}^{\mathrm{B}}\left(1+\frac{1}{c^2}(U-W_0)+\frac{1}{2}\frac{1}{c^2}v^2\right)\mathrm{d}\tau_{\mathrm{p}}\,.\end{aligned}$$

Since $\Delta t' \approx \Delta\tau_{\mathrm{p0}}$, the interval of proper time recorded by a clock at rest on the geoid, which corresponds to the interval of proper time recorded by a clock on the satellite, is therefore given by

$$\begin{aligned}\Delta\tau_{\mathrm{p0}} = &\left(1+\frac{3}{2}\frac{1}{c^2}\frac{GM_\oplus}{a}-\frac{1}{c^2}W_0\right)\Delta\tau_{\mathrm{p}}\\ &+\frac{2}{c^2}\sqrt{GM_\oplus a}\cdot e\sin E\,.\end{aligned} \tag{5.47}$$

It comprises a rate difference at the level of few parts in 10^{10} for common GNSS satellites as well as the eccentricity dependent periodic part with representative amplitudes of 10–100 ns. Both contributions and their practical implications for navigation satellite systems are further discussed in Sect. 5.4.5.

At the subnanosecond level of precision, it is necessary to take into account the orbital perturbations due to the harmonics of the Earth's gravitational potential, the tidal effects of the Moon and the Sun, as well as solar radiation pressure. Leading contributions result from the J_2 perturbation of the satellite position and velocity. Following [5.97], these give rise to a supplementary correction

$$\begin{aligned}\delta\Delta\tau_{\mathrm{p0}} = &\frac{7}{2}\frac{GM_\oplus R_\oplus^2}{a^3c^2}J_2\left(1-\frac{3}{2}\sin^2 i\right)\Delta\tau_{\mathrm{p}}\\ &-\frac{3}{2}\frac{R_\oplus^2}{a^2c^2}J_2\sqrt{GM_\oplus a}\sin^2 i\sin 2u\end{aligned} \tag{5.48}$$

that needs to be considered on top of (5.47). Here, i denotes the inclination of the satellite orbit while u is the argument of latitude. Besides a drift correction, the J_2 contribution comprises a harmonic term of about 0.1 ns amplitude with a twice-per-revolution periodicity.

To fully account for the J_2 perturbation in the potential of (5.36), it is necessary to perform a numerical integration of the orbit and a numerical integration of (5.42). The tidal effects of the Moon and the Sun and solar radiation pressure should also be considered. For low-Earth orbits, both the zonal and tesseral gravitational harmonics are important and the usual eccentricity correction of (5.46) is no longer accurate. In this case, it is likewise preferable to integrate the orbit and integrate (5.42) numerically including the higher-order harmonics of the Earth's gravitational potential.

Earth-Centered Earth-Fixed Coordinate System

Through terms of order $1/c^2$, the metric tensor components in the rotating Earth-centered Earth-fixed (ECEF) coordinate system are given by

$$\begin{aligned}-g_{00} &= 1-\frac{2U}{c^2}-\frac{||\boldsymbol{\omega}\times\boldsymbol{r}||^2}{c^2}\\ &= 1-\frac{2W}{c^2}\\ g_{0j} &= \frac{(\boldsymbol{\omega}\times\boldsymbol{r})_j}{c}\\ g_{ij} &= \delta_{ij}\,.\end{aligned} \tag{5.49}$$

Using coordinate time TT, the elapsed coordinate time is

$$\begin{aligned}\Delta t' = &\int_{\mathrm{A}}^{\mathrm{B}}\left(1-\frac{1}{c^2}gh+\frac{1}{2}\frac{1}{c^2}(v')^2\right)\mathrm{d}\tau_{\mathrm{p}}\\ &+\frac{1}{c^2}\int_{\mathrm{A}}^{\mathrm{B}}(\boldsymbol{\omega}\times\boldsymbol{r})\cdot\boldsymbol{v}'\mathrm{d}\tau_{\mathrm{p}}\,,\end{aligned} \tag{5.50}$$

where h is the height of the clock above the geoid, g is the local acceleration of gravity, v' is the velocity of the clock relative to the geoid, and $\boldsymbol{r}$ and $\boldsymbol{v}'$ are the position and velocity vectors of the clock in the ECEF frame. It is assumed that h is small. For high accuracy, the variation of g with latitude and elevation should also be taken into account.

The second integral of (5.50) is the Sagnac effect for a transported clock. This effect may be expressed as

$$\begin{aligned}\Delta t_{\mathrm{Sagnac}} &= \frac{1}{c^2}\int_{\mathrm{A}}^{\mathrm{B}}(\boldsymbol{\omega}\times\boldsymbol{r})\cdot\boldsymbol{v}'\mathrm{d}\tau_{\mathrm{p}}\\ &= \frac{1}{c^2}\int_{\mathrm{A}}^{\mathrm{B}}(\omega R_\oplus\cos\phi)(v'\cos\theta)\mathrm{d}\tau_{\mathrm{p}}\\ &= \frac{\omega R_\oplus^2}{c^2}\int_{\mathrm{A}}^{\mathrm{B}}\cos^2\phi\,\mathrm{d}\lambda = \frac{2\omega A}{c^2}\,,\end{aligned} \tag{5.51}$$

where ϕ is the latitude, λ is the longitude, $v' \cos\theta$ is the eastward component of the velocity, and A is the projection onto the equatorial plane of the area swept out by the position vector with respect to the center of the Earth (positive for the eastward direction and negative for the westward direction).

5.4.4 Propagation of Signals

This section deals with the computation of the coordinate time of propagation of signals when the transmitter and receiver positions are both given as expressed in the ECI, ECEF, and barycentric coordinate systems.

These equations apply in all cases. In particular, they must be used when setting the parameters of clocks on satellites that are steered to clocks on the Earth.

Propagation in ECI Coordinate System

When considering computation in an ECI coordinate system, the coordinate time of propagation (TCG) may be considered as the sum of a geometric part and a gravitational part. The geometric part is

$$\Delta t \approx \frac{1}{c} \int_{\text{path}} \sqrt{g_{ij} dx^i dx^j} = \frac{\rho}{c} , \tag{5.52}$$

where $g_{ij} \approx \delta_{ij}$ and ρ is the geometric path length of the signal path.

If the signal is transmitted at coordinate time t_T and is received at coordinate time t_R, the TCG of propagation over the path is

$$\begin{aligned} \Delta t = \frac{\rho}{c} &= \frac{1}{c} |\boldsymbol{r}_R(t_R) - \boldsymbol{r}_T(t_T)| \\ &\approx \frac{1}{c} |\Delta \boldsymbol{r} + \boldsymbol{v}_R(t_R - t_T)| \\ &\approx \frac{1}{c} |\Delta \boldsymbol{r}| + \frac{1}{c^2} \Delta(\boldsymbol{r} \cdot \boldsymbol{v}_R) , \end{aligned} \tag{5.53}$$

where the transmitter has position $\boldsymbol{r}_T$ and the receiver has position $\boldsymbol{r}_R$ and velocity $\boldsymbol{v}_R$ and where $\Delta \boldsymbol{r} \equiv \boldsymbol{r}_R(t_T) - \boldsymbol{r}_T(t_T)$ is the difference between the position of the receiver and the transmitter at the coordinate time of transmission t_T. The correction to the coordinate time due to the receiver velocity is

$$\Delta t_{\text{vel}} \approx \frac{\Delta \boldsymbol{r} \cdot \boldsymbol{v}_R}{c^2} . \tag{5.54}$$

Note that additional terms of order $1/c^3$ may amount to several picoseconds, depending on the configuration.

To consider the effect of the gravitational potential on an electromagnetic signal, it is necessary to include the potential in both the spatial and temporal parts of the metric. The components of the metric are

$$\begin{aligned} -g_{00} &= 1 - \frac{2U}{c^2} , \\ g_{0j} &= 0 , \\ g_{ij} &= \left(1 + \frac{2U}{c^2}\right) \delta_{ij} . \end{aligned} \tag{5.55}$$

Therefore, the elapsed TCG is

$$\begin{aligned} \Delta t &\approx \frac{1}{c} \int_{\text{path}} \sqrt{\frac{g_{ij}}{-g_{00}} dx^i dx^j} \\ &\approx \frac{1}{c} \left(1 + \frac{2U}{c^2}\right) \sqrt{\delta_{ij} dx^i dx^j} \\ &= \frac{\rho}{c} + \frac{1}{c^3} \int_{\text{path}} 2U \mathrm{d}\rho . \end{aligned} \tag{5.56}$$

The gravitational time delay is

$$\Delta t_{\text{delay}} = \frac{2GM_\oplus}{c^3} \ln\left(\frac{R + r + \rho}{R + r - \rho}\right) , \tag{5.57}$$

where R and r are the distances from the geocenter to the transmitter and receiver, respectively.

The gravitational delay typically amounts to a few tens of picoseconds for a path between a satellite and Earth. The total TCG is the sum of the terms in equations (5.53) and (5.57).

The coordinate time of propagation (TT) is

$$\begin{aligned} \Delta t' &= (1 - L_G) \Delta t \\ &= \frac{\rho}{c} - L_G \frac{\rho}{c} + \frac{2GM_\oplus}{c^3} \ln\left(\frac{R + r + \rho}{R + r - \rho}\right) . \end{aligned} \tag{5.58}$$

This is the time interval that would be measured by a clock on the geoid. For example, a signal sent from a geostationary satellite with orbital radius 42 164 km to a clock on the equator at the same longitude would have a path delay of −27 ps. For a GPS satellite at an elevation angle of 40°, the second and third terms nearly cancel so that the path delay is −3 ps.

Propagation in ECEF Coordinate System

When considering signal propagation in an ECEF coordinate system, the geometric part of the TCG is

$$\Delta t = \frac{1}{c} \int_{\text{path}} \sqrt{g_{ij} dx^i dx^j} + \frac{1}{c} \int_{\text{path}} g_{0j} \mathrm{d}x^j . \tag{5.59}$$

The metric components are

$$\begin{aligned} -g_{00} &\approx 1 \,, \\ g_{0j} &= \frac{(\boldsymbol{\omega} \times \boldsymbol{r})_j}{c} \,, \\ g_{ij} &\approx \delta_{ij} \,, \end{aligned} \tag{5.60}$$

where $\boldsymbol{r}$ is the position vector of a point on the signal path. The coordinate time (TT) is $\Delta t' = (1 - L_G)\Delta t$.

The first term of (5.59) is ρ'/c, where ρ' is the Euclidean path length in the ECEF coordinate system. If the transmitter has position $\boldsymbol{r}_T$ and the receiver has position $\boldsymbol{r}_R$ and velocity $\boldsymbol{v}'_R$, then

$$\begin{aligned} \frac{\rho'}{c} &= \frac{1}{c}|\boldsymbol{r}_R(t_R) - \boldsymbol{r}_T(t_T)| \\ &\approx \frac{1}{c}|\Delta\boldsymbol{r} + \boldsymbol{v}'_R(t_R - t_T)| \\ &\approx \frac{1}{c}|\Delta\boldsymbol{r}| + \frac{1}{c^2}\Delta\boldsymbol{r}\cdot\boldsymbol{v}'_R \,, \end{aligned} \tag{5.61}$$

where $\Delta\boldsymbol{r} \equiv \boldsymbol{r}_R(t_T) - \boldsymbol{r}_T(t_T)$.

The second term of (5.59) is the Sagnac effect. Therefore,

$$\begin{aligned} \Delta t_{\text{Sagnac}} &= \frac{1}{c^2}\int_A^B (\boldsymbol{\omega}\times\boldsymbol{r})\cdot\boldsymbol{v}'\,\mathrm{d}\tau_p \\ &= \frac{1}{c^2}\int_A^B (\boldsymbol{\omega}\times\boldsymbol{r})\cdot\mathrm{d}\boldsymbol{r} \\ &= \frac{1}{c^2}\int_A^B \boldsymbol{\omega}\cdot(\boldsymbol{r}\times\mathrm{d}\boldsymbol{r}) \\ &= 2\frac{1}{c^2}\int_A^B \omega\cdot\mathrm{d}A = \frac{2\omega A}{c^2} \,, \end{aligned} \tag{5.62}$$

where A is the projection onto the equatorial plane of the area formed by the center of rotation and the endpoints of the signal path. The gravitational delay must also be considered to compute the total time of propagation.

5.4.5 Relativistic Offset for GNSS Satellite Clocks

As noted before, the Global Positioning System as well as all other GNSSs must incorporate relativistic effects in their normal operation. They provide a means of performing time and position measurements with satellite clocks on a practical scale and a validation of the accuracy and consistency of the algorithms is used in such measurements across a broad area of applications.

For measurements with a precision at the nanosecond level, there are three relativistic effects that must be taken into account. First, there is the effect of time dilation. The velocity of a moving clock causes it to appear to run slow relative to a clock on the Earth. GPS satellites revolve around the Earth with an orbital period of 11.967 h and a velocity of 3.874 km/s. Thus, on account of its velocity, a GPS satellite clock appears to run slow by 7 μs/d. Second, there is the effect of gravitational redshift. At an altitude of 20 184 km the difference in gravitational potential causes the satellite clock to appear to run fast by 45 μs/d. In addition, the effects contributed by the velocity of rotation and gravitational potential of the rotating geoid must be included. The net effect of time dilation and gravitational redshift is that the satellite clock appears to run fast by approximately 38 μs/d when compared to a similar clock on the Earth's surface, which is an enormous rate difference for a clock with a precision of a few nanoseconds. To compensate for this large secular effect, the GPS clock is given a fractional rate offset prior to launch of $-4.465\cdot10^{-10}$ from its nominal frequency of exactly 10.23 MHz, so that on average it appears to run at the same rate as a clock on the ground. The actual frequency of the satellite clock prior to launch is thus 10.22999999543 MHz. Similar considerations apply for the other navigation satellite systems, even though the apparent frequency is different for each constellation due to the specific orbital altitude and velocity of the various satellites.

Although the GPS orbits are nominally circular, there is always some residual eccentricity. The eccentricity causes the orbit to be slightly elliptical. Thus the velocity and gravitational potential vary slightly over one revolution and, although the principal secular effect is compensated by a rate offset, there remains a small residual variation that is proportional to the eccentricity. For example, with an orbital eccentricity of 0.02, there is a relativistic sinusoidal variation in the apparent clock time having an amplitude of 46 ns at the orbital period. By convention [5.98], the eccentricity-dependent periodic relativistic effect is removed in precise clock products of all GNSSs produced by the IGS and other providers, to obtain an essentially linear variation of the reported clock offset. With the exception of GLONASS [5.99], the same holds for broadcast clock offset values transmitted by the various GNSSs as part of their navigation messages [5.100–104]. This correction must therefore be calculated and taken into account in the user's receiver.

The third relativistic effect is associated with the universality of the speed of light. Thus the displacement of the receiver relative to an inertial frame during the time of flight of the signal must be included. In the Earth's rotating frame of reference, this property is called the Earth rotation correction or Sagnac effect. For a receiver at rest on the rotating geoid observing a GPS satellite, the maximum correction is 133 ns.

GPS has served as a laboratory for doing physics at the one-to-ten nanosecond level. The consistent application of relativity to GPS Time and position measurements has been demonstrated by the operational precision of the system and by numerous experiments designed to test these individual effects over a wide range of conditions.

A more robust treatment of relativity will be required for clock modeling and orbit determination in future GNSS generations that are looking for greater accuracy. At the subnanosecond level, relativistic effects must be included that are not modeled in the present system. One of the most important comes from the contribution to the redshift from the gravitational potential harmonic due to Earth oblateness [5.97]. There is a secular effect of approximately 0.5 ns/day and a periodic effect at half the orbit period with amplitude of 0.04 ns (corresponding to about 1 cm). While partly masked by thermal clock or bias variations, this effect has become discernible with the high precision provided by modern rubidium or hydrogen maser clocks of new GNSS satellites [5.88]. At the few picosecond level, it is also necessary to consider the tidal potentials of the Sun and Moon and the Earth's gravitation has an effect on the speed of propagation of light itself. That is, the gravitational potential causes the speed of propagation to depart slightly from the value of c.

5.5 International Timescales

The development of atomic clocks and their use in GNSS has made precise and accurate clock measurements and comparisons available globally. One of the first applications of this technology was in the comparison and generation of global timescales. Since these clocks generate *atomic time*, their use in GNSS is linked to global timekeeping of atomic time and the accuracy of this timekeeping is now such that the principles of relativity need to be taken into account.

Atomic time has become the basis of all physically realized timescales. A version of atomic time has been maintained continuously in various laboratories since 1955 although not formally adopted as an international timescale until 1971. Prior to the creation of the Bureau International de l'Heure (BIH) in 1920 at the Paris Observatory, timescales were based wholly upon astronomical observations and were not internationally agreed. The unit of time of the timescale in use was the second and it was likewise based on the astronomical observation of the length of a day.

With advent and operation of cesium atomic standards in the 1950s, and broadcast systems such as Long Range Navigation (LORAN) enabling accurate international comparison of these standards, these led to the initial form of Atomic Time (AT). The formation of International Atomic Time (TAI) was recommended by the International Astronomical Union (IAU) in 1967, the International Union of Radio Science (URSI) in 1969 and the International Radio Consultative Committee (CCIR) of the International Telecommunication Union (ITU) in 1970.

The 14th General Conference on Weights and Measures (CGPM) approved the establishment of TAI in 1971 as the relativistic coordinate time scale whose unit interval is the second of the International System of Units (SI) as realized on the rotating geoid. This established the SI second as the standard for the unit of time based on the hyperfine frequency of cesium 133 [5.105, 106].

5.5.1 International Atomic Time (TAI)

The International Atomic Time (TAI) is the metrologic timescale maintained by the Bureau des Poids et Measure (BIPM) since timekeeping responsibility was transferred to the BIPM from the BIH in 1988 [5.24, 107]. It is established as the basis of atomic clock comparison data supplied to the BIPM by participating timekeeping centers and laboratories and is generated by a particular algorithm for treating the data known as ALGOS [5.108].

TAI is defined as a coordinate timescale in a geocentric reference frame with the SI second as the scale unit realized on the rotating geoid. The fact that TAI is a coordinate timescale was determined by the Consultative Committee for the Definition of the Second in 1980 and the necessary framework for evaluating the relativistic terms in the establishment of TAI have been presented in Sect. 5.4.

The accuracy of TAI is a primary consideration in maintaining the SI second and providing a reliable reference scale in the long term [5.109]. The optimization

of the long-term stability is done at the expense of short-term accessibility. The calculation of TAI uses data over an extended period. Clock-comparison data are sent to the BIPM every ten days on days with the modified Julian date (MJD) ending in 9. Blocks of data covering 60 days are used in the calculation of the scale.

A period of 60 days was chosen to place the effective integration time of the scale at the transition between the flicker floor and the random walk frequency modulation of cesium clocks. Stability would therefore not be improved by a longer integration time. The period of 60 days is enough to smooth out the noise contributed by the time links (GNSS and other comparison techniques) and the white frequency modulation noise of the clocks. The monthly BIPM Circular T then alternates between provisional, based on only 30 days of data, and the definite, based on the full 60 days of data.

The determination of TAI [5.110] is then performed in three steps:

1. Calculation (using a post-processing, iterative procedure) of an intermediate scale, known as Echelle Atomique Libre (EAL) or Free Atomic Scale, using the clock comparison data and ALGOS
2. The evaluation of the duration of the scale unit of EAL using data from primary frequency standards and an optimum filter
3. The production of TAI from EAL by applying, if necessary, a correction to the scale interval of EAL to give a value as close as possible to the SI second. Correcting of the scale unit is known as *steering* and is done infrequently.

At a time t, the free atomic time scale EAL is defined in terms of the readings $h_i(t)$ of the group of N clocks, H_i, contributed by the various timing centers, expressed as

$$\mathrm{EAL}(t) = \frac{\sum_{i=1}^{N} p_i [h_i(t) + h_i'(t)]}{\sum_{i=1}^{N} p_i} \,. \tag{5.63}$$

Here, p_i is the statistical weight assigned to clock H_i and $h_i'(t)$ is a time correction designed to ensure time and frequency continuity of the scale when either the weighting of individual clocks or the total number of clocks is changed [5.108, 111].

This expression cannot be used directly because the measured quantities that provide the basic data cannot be the readings of individual clocks but are comparisons between pairs of clocks. Such is the nature of timekeeping and clock measurements. At time t, the slowly varying differences $\zeta_{ij}(t)$ between clocks H_i and H_j are written as $\zeta_{ij}(t) = h_i(t) - h_j(t)$.

The output of EAL is N values of the differences $x_i(t)$ defined by $x_i(t) = \mathrm{EAL}(t) - h_i(t)$, where x_i are the differences between the individual clocks and the time defined by EAL. The difference can then be expressed as $x_i(t) - x_j(t) = -\zeta_{ij}(t)$, and (5.63) can be transformed into

$$\sum_{i=1}^{N} p_i x_i(t) = \sum_{i=1}^{N} p_i h_i'(t) \,. \tag{5.64}$$

In practice comparative data from the nonredundant system of $N-1$ time links between the timing centers is employed to solve for these last two expressions.

The weight assigned to each clock is calculated in such a way as to favor the long-term stability of the resulting scale. This also minimizes the annual fluctuations and frequency drift that the predominately commercial frequency standards maintained at the timing centers with respect to the primary timescale frequency standards. An important feature of the ALGOS algorithm is the fact that the evaluation of the weight of the clock, although based upon data covering a whole year, takes into account the 60 days of data for which EAL is being specifically computed. It is thus possible to judge clocks on their actual performance during the interval of time during which EAL is being established. It is also possible to take into account of any abnormal behavior observed in an individual clock by adjusting its weight, if necessary to zero. This has proved useful on many occasions.

The weight is normally based on the variance $\sigma_i^2(6,\tau)$ of mean rate with respect to EAL calculated over two-monthly samples [5.108]. This variance, instead of the usual pair variance, was chosen because it gives greater reduction in the weight of clocks showing a frequency drift. The weights are obtained directly from

$$p_i = \frac{1000}{\sigma_i^2(6,\tau)} \,, \tag{5.65}$$

with σ_i expressed in nanoseconds per day, provided that over the current period of 60 days no abnormal behavior is apparent. In the case of abnormal behavior a weight of zero is assigned. A maximum weight of 100 is assigned to the 15% or so of clocks having $\sigma_i(6,\tau) \le 3.16\,\mathrm{ns/d}$. The maximum weight is chosen to ensure that the scale is heavily biased in favor of the best clocks without allowing any one to become predominant, no clock having a contribution greater than about 2%.

The time correction term

$$h_i'(t) = a_i(t_0) + B_{ip}(t)(t - t_0) \tag{5.66}$$

is made up of two components, where $a_i(t_0)$ is simply the time differences between the clock H_i and EAL at a time t_0, which is the time at the beginning of the 60-day period, and $B_{ip}(t)$ is the predicted difference in rate between H_i and EAL for the period between t_0 and t. The rate of clock H_i, for example, is defined by

$$\text{rate} = \frac{a_i(t_0 - t) - a_i(t_0)}{t - t_0} \,. \tag{5.67}$$

The prediction of $B_{ip}(t)$ is obtained by a one-step linear prediction based upon the previous value. This is justified by the fact that the period of 60 days is such that the predominant clock noise is random walk for which the most probable estimate for the value over the next period is simply that over the immediate preceding period. Having established the best estimate of EAL the transformation to TAI is made by the decision whether or not the rate of EAL differs sufficiently from the rate of the best primary standards to warrant a correction or *steering*. From 1984 to 1989, no steering was necessary and thus during this period TAI was in fact simply EAL with a constant frequency offset. Since then, several frequency changes of five parts in 10^{15} each have been found necessary.

Finally, the output of these calculations is presented in the monthly *Circular T* published by the BIPM and distributed to participating timing centers. This circular is alternately provisional or definitive depending upon whether it is issued in the middle or at the end of a 60-day calculation period.

5.5.2 Coordinated Universal Time (UTC)

The initial form of atomic time attempted prior to 1972 was to keep close agreement to astronomical time by adjusting both the frequency offset and fractional step adjustments of time broadcasts of atomic time signals with the Earth's rotation. Close coupling to the Earth's rotation was considered necessary to aid celestial navigation, however that system of adjustment was very difficult to coordinate between broadcast stations and provide a uniform accurate reference time. The present UTC system was adapted so that an approximation to the epoch of universal time (UT1), a version of universal time (sometimes called mean solar time) that is determined by the transit time of stars corrected for seasonal variations, and the interval of the SI second would be provided by a single scale. The history and development of these timescales is discussed in [5.112].

The current definition of Coordinated Universal Time (UTC) was developed by the Consultative Committee for International Radiocommunication (CCIR; now known as International Telecommunications Union Radiocommunication sector, ITU-R) [5.110]. It was a compromise solution to the international timescale between using TAI and continuing international time based on the rotation of the Earth. It is a stepped atomic time scale based on the rate of TAI adjusted by the addition or deletion of integer seconds, known as leap seconds, to maintain the time within 0.9 s of Universal Time (UT1), UTC is used to coordinate the reference time kept by the timing centers. The specific definition is maintained by ITU-R Recommendation TF.460.6 [5.110, 113]. Since UTC was adopted its use has grown considerably within the radio and telecommunications community.

UTC is specifically defined as $\text{TAI} - \text{UTC} = n$, an integer number of seconds, and $|\text{UT1} - \text{UTC}| < 0.9\,\text{s}$. In 2014, UTC is behind TAI by 35 seconds. The integer number of seconds' difference is adjusted by the use of *leap seconds* (either positive or negative) to maintain the relationship of UTC to UT1. For other uses dependent upon coordination with Earth orientation the difference can be further refined by the additional term DUT1 recommended to be broadcast for further adjustment of UTC. DUT1 is the *predicted* difference, UT1–UTC in integral multiples of 0.1 s. A user of UT1 can then adjust the accuracy to < 0.1 s. The decision of when to insert a leap second is determined by the variable change in the rotation rate of the Earth. The International Earth Rotation and Reference Service (IERS) monitors the rotation rate of the Earth along with the other Earth orientation parameters including the predicted value of DUT1. They determine the need to adjust UTC and advise the BIPM when to insert or delete the second.

As the needs of GNSS operations, broadcasting and timekeeping services require the generation and transmission of a *real-time* or immediate timescale and UTC itself is based on the rate of TAI which is a post-processed metrologic timescale, a real-time version was needed. This real-time version also needed to be produced from the same clocks and oscillators that produce the timekeeping data for TAI. To provide a real-time timescale timing centers produce a real-time representation of UTC and identify it by using the nomenclature UTC(k) where k is the timing center. UTC without the qualifying parentheses and k nomenclature would then identify the timescale referenced as the final international value determined by the BIPM. The centers maintaining a realization of UTC relating to the major GNSS and their values of UTC(k) are shown in Fig. 5.32.

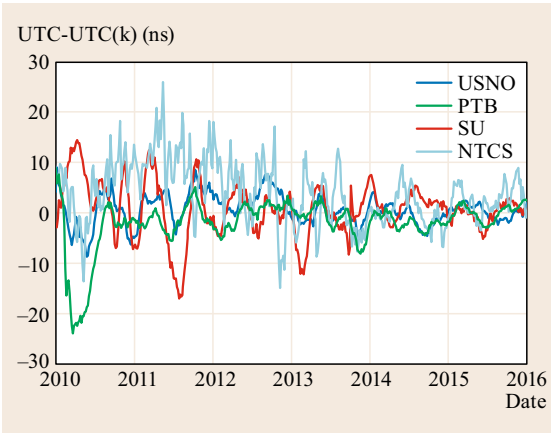

Fig. 5.32 Values of UTC(k) realizations of UTC maintained by associated GNSS timing centers (after [5.114])

These qualifications are made in ITU-R Recommendation TF.536 on Time-Scale Notation [5.115]. The final determination of UTC does not have a physical output and is available after a delay of two to four weeks in the form of an offset from the representation maintained by a participating laboratory. The value for both TAI and UTC are disseminated by the BIPM via the monthly publication of *Circular T*. The offset of TAI and UTC with respect to participating observatories or laboratories is given in terms of TAI or UTC minus UTC(k). For example, UTC (USNO) is the delivered real-time prediction of UTC as maintained by US Naval Observatory.

UTC is recognized as the basis of global timekeeping and telecommunications use and is the only timescale that is physically realized and disseminated. The CCIR in 1978 and the World Administrative Radio Conference (Geneva) in 1979 recommended that UTC should be used to designate the time in all international telecommunication activities. The ITU *Radio Regulations* define UTC as the timescale based on the SI second, specified in Recommendation ITU-R TF.460, and notes that UTC may be regarded as the general equivalent of mean solar time at the Greenwich meridian. The global reference for GNSS and satellite time and frequency applications is UTC. Its use in GNSS and managing with its discontinuous nature will be discussed in the following sections.

5.6 GNSS Timescales

In order to achieve synchronicity within a GNSS a stable common time reference must be globally available for the supporting ground segment to provide precise observations of the satellites for computation of the data products needed to operate the system and support the many users. This time reference is most commonly achieved in today's GNSSs through generation of its own real-time internal timescale in each system. Classically, reference time for a system was provided by establishing a specific master clock whose signals were transmitted or distributed as the reference time for all system measurements. For a system of global extent this master clock approach is difficult. It is virtually the same problem as global timekeeping but on a real-time basis.

The approach developed to address this problem is to generate an internal timescale in real time that is in effect a virtual system timescale made from the measurements of the clocks within the system. The system timescale is therefore not physically realized by an actual clock output within the system. This virtual time reference is possible since the GNSS must be supported by a global network of tracking sites to track and provide data to a centralized site in real time. Here, *real-time* means that as the observational data is collected the system data is incrementally generated for the system. The computation of the satellite ephemerides and other navigation-related data, including the clock parameters of the satellites and ground supporting network, may be determined against a weighted average of the clock observed values.

The internal system reference timescale, GPS Time (GPST) for example, is produced in this manner. The process is similar to that of the international timescale being a weighted ensemble average of the physical clocks contributing to the operation of the system. Whereas the product of the international timescale is the publication of the offsets of the contributing time centers after the fact, a GNSS must have a real-time determination of the time within the system as the basis of system position and timing measurements. Consequently, the technique adopted has been the generation of a real-time weighed ensemble of the system's internal clocks that results in a time reference that is only physically realized by the clock output of the system's user receivers. The significant difference between the international timescale and the internal time reference is not just the real-time condition but the fact that the system time reference must deal with clocks of different characteristics. Classical ensembling for timescales deals with the same kind or similar clocks. With dissimilar types the combination of their stochastic characteristics has more complex computational difficulties.

An alternative approach to generating an internal system time reference is the more classical approach of considering the time reference to be independent of the system. Computationally the system's parameters would then consider time to be an independent value. The satellite and ground clocks could be monitored and maintained independently of the internal system operations through direct measurements of each clock, satellite or ground, using techniques such as two-way satellite time and frequency transfer (TWSTFT). This two-way technique is more commonly employed with communication satellites to compare clocks at ground sites but could be employed within a GNSS [5.116]. However, maintaining the clocks independently would lose the computational correlations with the other system parameters such as the satellite ephemerides since the precision and accuracy of the system measurements to the reference issue still needs to be minimized.

Consequently, within an internal time reference, observations are gathered passively and processed by the use of models, environmental measurements and other means of compensation of relevant observation effects necessary to relate the clocks to one another. A clock error model and timescale algorithm is then applied to the clock differences to produce estimates of the error of each clock relative to a stable virtual system timescale. Offset corrections of each satellite relative to its reference are then transmitted from each satellite in the form of predictions of the clock relative to System Time (ST) as part of its navigation message, along with the epoch of the prediction parameters so that offsets may be determined by the receiver software relative to the current epoch.

Variations of this approach are utilized by all of the major GNSSs, including GPS, GLONASS, Galileo, and BeiDou. Additional predicted corrections that relate the GNSS timescale to that of other systems and to UTC maintained by the timekeeping center associated with the particular system are also transmitted in the satellite system messages. Note that the GNSS ground segment upload interval for predicted navigation data to be transmitted by the satellites is primarily determined by the intrinsic stability of the satellite clocks. The more stable the satellite clock the less frequent an upload of the predicted clock corrections is necessary. For example, GPS satellites navigation uploads and clock prediction corrections in the 2015 time period are nominally once per day.

Table 5.2 summarizes the current relationship between each of the main quartet of GNSS times and UTC as well as the system's strategy for maintaining time. All system times except GLONASS Time are continuous timescales that do not apply leap seconds as are currently applied to UTC.

GNSS receivers that are capable of simultaneously tracking satellites from multiple GNSSs are increasingly available. Because each system provides corrections relative to its own internal ST the user of multi-GNSS signals must either sacrifice the additional degrees of freedom necessary to estimate the offsets between each GNSS ST or, where available, utilize any cross-GNSS offsets that are may be included in the navigation messages.

In the case of GPST, each GPS satellite carries multiple atomic clocks, however only one is used to generate the satellite transmissions at a time. The satellite clocks and monitor station clocks contribute to the statistical formation of the continuous system time known as GPS Time [5.117, 118], which is specified to be within 1 μs of UTC(USNO) modulo leap seconds since leap seconds are not inserted in GPS Time. GPST provides a time reference typically at a precision of better than 25 ns. However, depending upon the receiving equipment used in practice the precision can be 20 ns or better.

The epoch of GPST is midnight of January 5/6, 1980 UTC. Therefore, GPST is behind TAI by a constant value of 19 s. As of the beginning of 2016, GPST is ahead of UTC by 17 s which changes every time a leap second is applied to UTC. GPST is optimized for the navigation service, which requires short-term stability and uniform global distribution. For timing ap-

Table 5.2 GNSS Times versus UTC for the main quartet of GNSSs. Each offset is separated into the whole number of seconds and its subsecond component C_i. Furthermore, $n = \text{TAI} - \text{UTC}$ denotes the integer second offset between International Atomic Time and Coordinated Universal Time (e.g., $n = 36$ s starting on 1 July 2015)

UTC – GPST	$0\,\text{h} - n + 19\,\text{s} + C_0$	GPS Time (GPST) is steered to UTC(USNO), C_0 is required to be less than 1 μs but is typically less than 20 ns
UTC – GLST	$-3\,\text{h} + 0\,\text{s} + C_1$	GLONASST (GLONASS Time) is steered to UTC(SU) including leap seconds. C_1 is required to be less than 1 ms. Note that GLONASST is offset from UTC by −3 hours corresponding to the offset of Moscow local time from the Greenwich meridian.
UTC – GST	$0\,\text{h} - n + 19\,\text{s} + C_2$	Galileo Time (GST) is steered to a set of European Union UTC(k) realization and C_2 is nominally less than 50 ns.
UTC – BDT	$0\,\text{h} - n + 33\,\text{s} + C_3$	BeiDou Time (BDT) is steered to UTC(NTSC) and C_3 is specified to be maintained less than 100 ns.

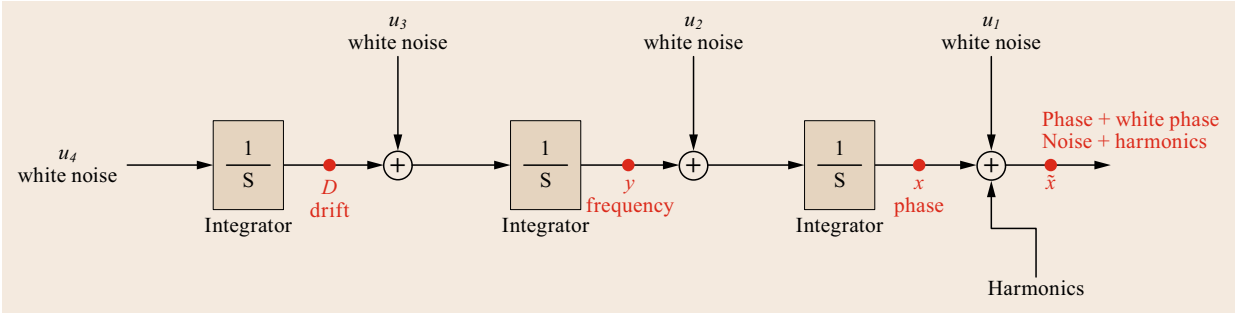

Fig. 5.33 IGS v2.0 Clock Model

plications that require a source of UTC, the real-time predicted offset of UTC (as realized at USNO) with respect to GPS Time is available from the GPS broadcast navigation message [5.100].

Like GPS, Galileo has adopted a uniform system time (GST) that does not contain leap seconds [5.101]. The starting epoch for GST is 00:00 on 22 August 1999 UTC (midnight between 21 and 22 August 1999). At this starting epoch GST was set to be ahead of UTC by 13 seconds so as to be consistent with GPST. The epoch for the Chinese BeiDou navigation satellite system time (BDT) is 00:00 on 1 January 2006 UTC and is related to UTC through UTC(NTSC) [5.102].

A primary requirement for a satellite navigation system is a uniformly precise system of time so that the navigation service is not interrupted by adjusting clocks. Such has not been the case with the Russian GLONASS satellite navigation system, which uses UTC(SU) offset by three hours as its system time [5.99].

The International GNSS Service (IGS; Chap. 33) established by the geodetic community also determines their own observational timescale, known as IGS Time (IGST) for coherency of the measurement data collected globally by numerous agencies and sites. Its formation is similar to GPST [5.119, 120]. The clock model used in the second version of IGST implemented in 2011 [5.121] uses a basic four-state model for all the clocks, which is illustrated in Fig. 5.33.

The base model contains a deterministic phase x, the phase derivative (frequency) y, and the second derivative D of phase (drift) each with an independent random walk component. An additional phase state $\tilde{x}$ is included to model a pure white phase noise and to couple it to any harmonic states. In accord with the observed clock behavior discussed in Sect. 5.3.6 four additional state parameters a_{ω_1}, b_{ω_1}, a_{ω_2} and b_{ω_2} are used to model up to two (once- and twice-per-revolution) harmonics that can appear in the satellite observations.

Acknowledgments. The authors would like to thank Dr. Joseph White, a colleague at the US Naval Research Laboratory, as well as Dr. Bob Nelson. Publication restrictions did not permit including Dr. White or Dr. Nelson in the authorship though many of the sections on individual atomic frequency standards and relativity were either contributed or edited by them.

References

5.1 D.B. Sullivan, D.W. Allan, D.A. Howe, F.L. Walls: *Characterization of Clocks and Oscillators*, TN-1337 (US National Institute of Standards and Technology, Gaithersburg 1990)

5.2 D.A. Howe, D.W. Allan, J.A. Barnes: Properties of signal sources and measurement methods, Proc. 35th Annu. Symp. Freq. Contr., Ft. Monmouth (IEEE, Piscataway 1981) pp. 669–716

5.3 J. Rutman, F.L. Walls: Characterization of frequency stability in precision frequency sources, Proc. IEEE **79**(7), 952–960 (1991)

5.4 T. Walter: Characterizing frequency stability: A continuous power-law model with discrete sampling, IEEE Trans. Instrum. Meas. **43**(1), 69–79 (1994)

5.5 W.J. Riley: *Handbook of Frequency Stability Analysis*, NIST Special Publication, Vol. 1065 (US National Institute of Standards and Technology, Gaithersburg 2008)

5.6 J.A. Barnes, A.R. Chi, L.S. Cutler, D.J. Healey, D.B. Leeson, T.E. McGunigal, J.A. Mullen Jr., W.L. Smith, R.L. Sydnor, R.F.C. Vessot, G.M.R. Winkler: Characterization of frequency stability, IEEE Trans. Instrum. Meas. **IM-20**(2), 105–120 (1971)

5.7 S.R. Stein: Frequency and time – Their measurement and characterization. In: *Precision Frequency Control*, Vol. 2, ed. by E.A. Gerber, A. Ballato (Academic Press, New York 1985) pp. 191–232

5.8 M.E. Frerking: Fifty years of progress in quartz crystal frequency standards, Proc. 50th IEEE Freq. Contr. Symp., Honolulu (1996) pp. 33–46

5.9 W.L. Smith: Quartz frequency standards and clocks – Frequency standards in general. In: *Precision Frequency Control*, Vol. 2, ed. by E.A. Gerber, A. Ballato (Academic Press, New York 1985) pp. 79–89

5.10 Hewlett-Packard: Fundamentals of Quartz Oscillators, Application Note 200-2 Electronic Counter Series (Hewlett-Packard Company, Palo Alto 1997)

5.11 C.S. Lam: A review of the recent development of MEMS and crystal oscillators and their impacts on the frequency control products industry, IEEE Ultrason. Symp., Beijing (IEEE, New Jersey 2008) pp. 694–704

5.12 J. Vanier, C. Audoin: Rubidium frequency standards. In: *The Quantum Physics of Atomic Frequency Standards*, Vol. 2, (Adam Hilger, Bristol 1989) pp. 1259–1350

5.13 S. Leschiutta: The definition of the 'atomic' second, Metrologia **42**, S10–S19 (2005)

5.14 *The International System of Units (SI)*, 8th edn. (Bureau International des Poids et Mesures, Paris 2006)

5.15 J. Vanier, C. Audoin: Cesium beam frequency standard, Part 1: Basic principles, frequency stability. In: *The Quantum Physics of Atomic Frequency Standards*, Vol. 2, ed. by EDITOR (Adam Hilger, Bristol 1989) pp. 613–781

5.16 A. Bauch: Caesium atomic clocks: Function, performance and applications, Meas. Sci. Technol. **14**(8), 1159–1173 (2003)

5.17 D. Kleppner, H.M. Goldenbergand, N.F. Ramsey: Theory of the hydrogen maser, Phys. Rev. **126**(2), 603–615 (1962)

5.18 D. Kleppner, H.C. Berg, S.B. Crampton, N.F. Ramsey, R.F.C. Vessot, H.E. Peters, J. Vanier: Hydrogen-maser principles and techniques, Phys. Rev. **138**(4A), A972–A983 (1965)

5.19 D.A. Howe, F.L. Walls, H.E. Bell, H. Hellwig: A small, passively operated hydrogen maser, Proc. 33rd Annu. Symp. Freq. Contr., Atlantic City (1979) pp. 554–562

5.20 H.T.M. Wang: An oscillating compact hydrogen maser, Proc. 34th Annu. Symp. Freq. Contr., Philadelphia (1980) pp. 364–369

5.21 W.M. Golding, R. Drullinger, A. De Marchi, W. Phillips: An atomic fountain frequency standard at NIST, Proc. 5th Symp. Freq. Stand. Metrol., Woods Hole, ed. by J.C. Bergquist (World Scientific, Singapore 1995) pp. 5–10

5.22 S.R. Jefferts, J. Shirley, T.E. Parker, T.P. Heavner, D.M. Meekhof, C. Nelson, F. Levi, G. Costanzo, A. De Marchi, R. Drullinger, L. Hollberg, W.D. Lee, F.L. Walls: Accuracy evaluation of NIST-F1, Metrologia **39**, 321–326 (2002)

5.23 R. Wynands, S. Weyers: Atomic fountain clocks, Metrologia **42**, s64–s79 (2005)

5.24 E.F. Arias: The metrology of time, Phil. Trans. R. Soc. A **363**, 2289–2305 (2005)

5.25 H.J. Metcalf, P. van de Straten: *Laser Cooling and Trapping* (Springer, New York 1999) pp. 156–164

5.26 M.A. Lombardi, T.P. Heavner, S.R. Jefferts: NIST primary frequency standards and the realization of the second, NCSL Int. Meas. **2**(4), 74–89 (2007)

5.27 S.L. Rolston, W.D. Phillips: Laser cooled neutral atom frequency standards, Proc. IEEE **79**(7), 943–951 (1991)

5.28 L. Cacciapuoti, C. Salomon: Atomic clock ensemble in space, J. Phys. Conf. Ser. **327**(012049), 1–13 (2011)

5.29 J. Vanier, A. Godone, F. Levi, S. Micalizio: Atomic clocks based on coherent population trapping: Basic theoretical models and frequency stability, Proc. IEEE FCS 17th EFTF 2003, Tampa (2003) pp. 2–15

5.30 R. Lutwak, A. Rushed, M. Varghese, G. Tepolt, J. Lablanc, M. Mescher, D.K. Serkland, G.M. Peake: The miniature atomic clock – Preproduction results, Proc. IEEE FCS 21st EFTF 2007, Geneva (2007) pp. 1327–1333

5.31 F.-C. Chan, M. Joerger, S. Khanafseh, B. Pervan, O. Jakubov: Reducing the jitters – How a chip-scale atomic clock can help mitigate broadband interference, GPS World **5**(25), 44–51 (2014)

5.32 V. Giordano, S. Grop, B. Dubois, P.-Y. Bourgeois, Y. Kersalé, G. Haye, V. Dolgovskiy, N. Bucalovic, G. Di Domenico, S. Schilt, J. Chauvin, D. Valat, E. Rubiola: New generation of cryogenic sapphire microwave oscillators for space, metrology and scientific applications, Rev. Sci. Instrum. **83**(085113), 1–6 (2012)

5.33 E.A. Burt, S. Taghavi-Larigani, J.D. Prestage, R.L. Tjoelker: Compensated multi-pole mercury trapped ion frequency standard and stability evaluation of systematic effects, Proc. 7th Symp. Freq. Stand. Metrol., Pacific Grove, ed. by L. Maleki (World Scientific, Singapore 2009) pp. 321–328

5.34 N. Poli, C.W. Oates, P. Gill, G.M. Tino: Optical atomic clocks, Riv. Nuovo Cimento **36**(12), 555–624 (2013)

5.35 A.G. Smart: Optical-lattice clock sets new standard for timekeeping, Phys. Today **63**(3), 12–14 (2014)

5.36 J. Ye, H. Schnatz, L. Hollberg: Optical frequency combs: From frequency metrology to optical phase control, IEEE J. Quantum Electron. **9**(4), 1041–1058 (2003)

5.37 T.A. Stansell: The navy navigation satellite system: Description and status, Navigation **15**(3), 229–243 (1968)

5.38 B.W. Parkinson, T.A. Stansell, R.L. Beard, K. Gromov: A history of satellite navigation, Navigation **42**(1), 109–164 (1995)

5.39 R.L. Beard, J.A. Murray, J.D. White: GPS clock technology and navy PTTI programs at the US Naval research laboratory, Proc. 18th Annu. PTTI Meet., Reston (1987) pp. 37–53

5.40 A.B. Bassevich, P. Bogdanov, A.G. Gevorkyan, A. Tyulyakov: Glonass onboard time/frequency standards: Ten years of operation, Proc. 28th Annu. PTTI Meet., Reston (1997) pp. 455–462

5.41 R. Fatkulin, V. Kossenko, S. Storozhev, V. Zvonar, V. Chebotarev: GLONASS space segment: Satellite constellation, GLONASS-M and GLONASS-K spacecraft, main features, ION GNSS 2012, Nashville (2012) pp. 3912–3930

5.42 P. Rochat, F. Droz, P. Mosset, G. Barmaverain, Q. Wang, D. Boving, L. Mattioni, M. Belloni,

M. Gioia, U. Schmidt, T. Pike, F. Emma: The on-board galileo rubidium and passive maser, status and performance, Proc. IEEE FCS 2005, Vancouver (2005) pp. 26–32
5.43 J. Xie: Study to spaceborne rubidium atomic clocks characteristics and ground test requirements, Proc. CSNC 2014, Nanjing, Vol. III, ed. by J. Sun, W. Jiao, H. Wu, M. Lu (Springer, Berlin 2014) pp. 451–461
5.44 C. Li, T. Yang, L. Zhai, L. Ma: Development of new-generation space-borne rubidium clock, Proc. CSNC 2013, Wuhan, Vol. III, ed. by J. Sun, W. Jiao, H. Wu, C. Shi (Springer, Berlin 2013) pp. 379–386
5.45 Y. Xie, P. Chen, S. Liu, T. Pei, Y. Shuai, C. Lin: Development of space mini passive hydrogen maser, Proc. CSNC 2015, Xi'an, Vol. III, ed. by J. Sun, J. Liu, S. Fan, X. Lu (Springer, Berlin 2015) pp. 343–349
5.46 N.D. Bhaskar, J. White, L. Mallette, T. McClelland, J. Hardy: A historical review of atomic frequency standards used in space systems, Proc. 50th IEEE FCS, Honolulu (1996) pp. 24–32
5.47 L. Mallette, J. White, P. Rochat: Space qualified frequency sources (clocks) for current and future GNSS applications, IEEE/ION PLANS 2010, Indian Wells (2010) pp. 903–908
5.48 J. White, R. Beard: Space clocks – Why they're different, Proc. 33rd PTTI Meet., Long Beach, ed. by L.A. Breakiron (USNO, Washington, DC 2001) pp. 7–18
5.49 S. Nichols, J.D. White, F. Danzy: *Design and Ground Test of the NTS1 Frequency Standard System*, Naval Research Laboratory Report 7904, (Naval Research Laboratory, Washington 1975)
5.50 C.O. Alley, R. Williams, G. Singh, J. Mullendore: Performance of the new Efratom optically pumped rubidium frequency standards and their possible application in space relativity experiments, Proc. 4th PTTI Plan. Meet., Greenbelt (1972) pp. 29–40
5.51 M.J. Van Melle: Cesium and rubidium frequency standards status and performance on the GPS program, Proc. 27th Annu. PTTI Meet., San Diego (1996) pp. 167–180
5.52 W.J. Riley: A rubidium clock for GPS, Proc. 13th Annu. PTTI Meet., Washington (1982) pp. 609–630
5.53 F. Vannicola, R.L. Beard, J.D. White, K. Senior, M. Largay, J.A. Buisson: GPS block IIF atomic frequency standard analysis, Proc. 42nd Annu. PTTI Meet., Reston (2011) pp. 181–196
5.54 R.T. Dupuis, T.J. Lynch, J.R. Vaccaro, E.T. Watts: Rubidium frequency standard for the GPS IIF program and modifications for the RAFSMOD program, Proc. ION GNSS 2010, Portland (2010) pp. 781–788
5.55 Y.G. Gouzhva, A.G. Gevorkyan, V.V. Korniyenko: Atomic frequency standards for satellite radio navigation systems, Proc. 45th IEEE FCS, Los Angeles (1991) pp. 591–593
5.56 F. Droz, P. Rochat, Q. Wang: Performance overview of space rubidium standards, Proc. 24th EFTF, Noordwijk (2010) pp. 1–6
5.57 P. Waller, F. Gonzalez, S. Binds, I. Sesia, I. Hidalgo, G. Tobias, P. Tavella: The in-orbit performance of GIOVE clocks, IEEE Trans. Ultrason. Ferroelectr. Freq. Contr. **57**(3), 738–745 (2010)
5.58 J.D. White, F. Danzy, S. Falvey, A. Frank, J. Marshall: NTS-2 cesium beam frequency standard for GPS, Proc. 8th Annu. PTTI Meet., Washington (1977) pp. 637–664
5.59 Symmetricom: *Datasheet 4415 Digital Cesium Frequency Standard* (Symmetricom, San Jose 2003)
5.60 S. Feairheller, J. Purvis, R. Clark: The Russian GLONASS system. In: *Understanding GPS – Principles and Applications*, ed. by E.D. Kaplan (Arctech House, Boston, London 1996) pp. 439–465
5.61 Y.G. Gouzhva, A.G. Gevorkyan, A.B. Bassevich, P.P. Bogdanov, A.Y. Tyulyakov: Comparative analysis of parameters of GLONASS spaceborne frequency standards when used onboard and on service life tests, Proc. 47th IEEE FCS, Salt Lake City (1993) pp. 65–70
5.62 A. Bassevich, B. Shebshaevich, A. Tyulyakov, V. Zholnerov: Onboard atomic clocks GLONASS: Current status and future plans, Proc. ION GNSS 2007, Sess. F6a, Fort Worth (2007) pp. 1–11
5.63 R.F.C. Vessot, M.W. Levine: A test of the equivalence principle using a space-borne clock, Gen. Relat. Gravit. **10**, 181–204 (1979)
5.64 R.L. Easton: The hydrogen maser program for NAVSTAR GPS, Proc. 8th Annu. PTTI Meet., Washington (1976) pp. 3–12
5.65 J.D. White, A.F. Frank, V.J. Folen: Passive maser development at NRL, Proc. 12th Annu. PTTI Meet., Greenbelt (1981) pp. 495–514
5.66 H.T.M. Wang: Subcompact hydrogen maser atomic clocks, Proc. IEEE **77**(7), 982–992 (1989)
5.67 L. Mattioni, M. Belloni, P. Berthoud, I. Pavlenko, H. Scheda, Q. Wang, P. Rochat, F. Droz, P. Mosset, H. Ruedin: The development of a passive hydrogen maser clock for the galileo navigation system, Proc. 34th Annu. PTTI Meet., Reston (2003) pp. 161–170
5.68 P. Berthoud, I. Pavlenko, Q. Wang, H. Schweda: The engineering model of the space passive hydrogen maser for the European global navigation satellite system Galileo, Proc. IEEE FCS 17th EFTF 2003, Tampa (2003) pp. 90–94
5.69 Q. Wang, P. Mosset, F. Droz, P. Rochat, G. Busca: Verification and optimization of the physics parameters of the onboard Galileo passive hydrogen maser, Proc. 38th Annu. PTTI Meet., Reston (2007) pp. 81–94
5.70 A. Jornod, D. Goujon, D. Gritti, L.G. Bernier: The 35 kg space active hydrogen maser (SHM-35) for ACES, Proc. IEEE FCS 17th EFTF 2003, Tampa (2003) pp. 82–85
5.71 D. Goujon, P. Rochat, P. Mosset, D. Boving, A. Perri, J. Rochat, N. Ramanan, D. Simonet, X. Vernez, S. Froidevaux, G. Perruchoud: Development of the space active hydrogen maser for the ACES mission, Proc. 24th EFTF, Noordwijk (2010) pp. 1–6
5.72 J.D. Prestage, S. Chung, T. Le, M. Beach, L. Maleki, R.L. Tjoelker: One-liter Hg ion clock for space and ground applications, Proc. IEEE FCS 17th EFTF 2003, Tampa (2003) pp. 1089–1091
5.73 R.L. Tjoelker, J.D. Prestage, L. Maleki: The JPL Hg+ extended linear ion trap frequency standard: Status, stability, and accuracy prospects, Proc. 28th

Annu. PTTI Meet., Reston (1997) pp. 245–254
5.74 T. Ely, J. Seubert, J. Bell: Advancing navigation timing, and science with the deep space atomic clock, SpaceOps 2014 Conf., Pasadena (AIAA, Reston 2014) pp. 1–19
5.75 F.J. Gonzalez Martinez: Performance of New GNSS Satellite Clocks, Ph.D. Thesis (Karlsruher Institut für Technologie, Karlsruhe 2013)
5.76 A. Baker: GPS Block IIR time standard assembly architecture, Proc. 22rd Annu. PTTI Meet., Vienna (1991) pp. 317–324
5.77 H. Rawicz, M. Epstein, J. Rajan: The time keeping system for GPS block IIR, Proc. 24th Annu. PTTI Meet., McLean (1993) pp. 5–16
5.78 A. Wu: Performance evaluation of the GPS block IIR timekeeping system, Proc. 28th Annu. PTTI Meet., Reston, ed. by L. Breakiron (USNO, Washington 1997) pp. 441–453
5.79 F.J.M. Carrillo, A.A. Sanchez, L.B. Alonso: Hybrid synthesizers in space: Galileo's CMCU, Proc. 2nd Int. Conf. Recent Adv. Space Technol., Istanbul (2005) pp. 361–368
5.80 D. Felbach, D. Heimbuerger, P. Herre, P. Rastetter: Galileo payload 10.23 MHz master clock generation with a clock monitoring and control unit (CMCU), Proc. IEEE FCS 17th EFTF 2003, Tampa (2003) pp. 583–586
5.81 D. Felbach, F. Soualle, L. Stopfkuchen, A. Zenzinger: Clock monitoring and control units for navigation satellites, Proc. IEEE FCS 2010, Newport Beach (2010) pp. 474–479
5.82 K. Kovach: New user equivalent range error (UERE) budget for the modernized Navstar Global Positioning System (GPS), Proc. ION NTM 2000, Anaheim (ION, Virginia 2000) pp. 550–573
5.83 J. Oaks, M. Largay, J. Buisson, W. Reid: Comparative analysis of GPS clock performance using both code phase and carrier derived pseudorange observations, Proc. 36th Annu. PTTI Syst. Appl. Meet., Washington (2004) pp. 431–440
5.84 J. Ray, K. Senior: Geodetic techniques for time and frequency comparisons using GPS phase and code measurements, Metrologia **42**, 215–232 (2005)
5.85 Z. Deng: Reprocessing of GFZ Multi-GNSS product GBM, IGS Workshop 2016, Sydney (IGS, Pasadena 2016)
5.86 F. Gonzalez, P. Waller: GNSS clock performance analysis using one-way carrier phase and network methods, Proc. 39th Annu. PTTI Meet., Long Beach (ION, Virginia 2007) pp. 403–414
5.87 J. Delporte, C. Boulanger, F. Mercier: Simple methods for the estimation of the short-term stability of GNSS on-board clocks, Proc. 42nd Annu. PTTI Appl. Plan. Meet., Reston (ION, Virginia 2010) pp. 215–223
5.88 O. Montenbruck, P. Steigenberger, E. Schönemann, A. Hauschild, U. Hugentobler, R. Dach, M. Becker: Flight characterization of new generation GNSS satellite clocks, Navigation **59**(4), 291–302 (2012)
5.89 A. Hauschild, O. Montenbruck, P. Steigenberger: Short-term analysis of GNSS clocks, GPS Solut. **17**(3), 295–307 (2013)
5.90 E. Griggs, E.R. Kursinski, D. Akos: Short-term GNSS satellite clock stability, Radio Sci. **50**(8), 813–826 (2015)
5.91 E. Griggs, E.R. Kursinski, D. Akos: An investigation of GNSS atomic clock behavior at short time intervals, GPS Solut. **18**(3), 443–452 (2014)
5.92 J.E. Gray, D.W. Allan: A method for estimating the frequency stability of an individual oscillator, Proc 8th Annu. Symp. Freq. Contr., Fort Monmouth (Electronic Industries Association, Washington 1974) pp. 277–287
5.93 K. Senior, J. Ray, R.L. Beard: Characterization of periodic variations in the GPS satellite clocks, GPS Solut. **12**(3), 211–225 (2008)
5.94 O. Montenbruck, U. Hugentobler, R. Dach, P. Steigenberger, A. Hauschild: Apparent clock variations of the block IIF-1 (SVN-62) GPS satellite, GPS Solut. **16**(3), 303–313 (2012)
5.95 O. Montenbruck, P. Steigenberger, U. Hugentobler: Enhanced solar radiation pressure modeling for Galileo satellites, J. Geod. **89**(3), 283–297 (2015)
5.96 G. Petit, B. Luzum: *IERS Conventions (2010)*, IERS Technical Note No. 36 (Verlag des Bundesamts für Kartographie und Geodäsie, Frankfurt 2010)
5.97 J. Kouba: Improved relativistic transformations in GPS, GPS Solut. **8**(3), 170–180 (2004)
5.98 J. Kouba: *A Guide to Using International GNSS Service (IGS) Products* (IGS, Pasadena 2015), http://kb.igs.org/
5.99 Russian Institute of Space Device Engineering: *Global Navigation Satellite System GLONASS – Interface Control Document*, Vol. 5.1 (Russian Institute of Space Device Engineering, Moscow 2008)
5.100 Global Positioning Systems Directorate: *Navstar GPS Space Segment/Navigation User Segment Interfaces, Interface Specification*, IS-GPS-200H, 24 Sep. 2013 (Global Positioning Systems Directorate, Los Angeles Air Force Base, El Segundo 2013)
5.101 European GNSS (Galileo) Open Service Signal In Space Interface Control Document, OS SIS ICD, Iss. 1.1, Sep. 2010 (EU 2010)
5.102 China Satellite Navigation Office: *BeiDou Navigation Satellite System Signal In Space Interface Control Document – Open Service Signal*, v2.0, Dec. 2013 (China Satellite Navigation Office, Bejing 2013)
5.103 JAXA: Quasi-Zenith Satellite System Navigation Service Interface Specification for QZSS, IS-QZSS, V1.4, 28 Feb. 2012 (JAXA, Chōfu 2012)
5.104 Indian Space Research Organization: *Indian Regional Navigation Satellite System – Signal In Space ICD for Standard Positioning Service*, version 1.0, June 2014 (Indian Space Research Organization, Bangalore, 2014)
5.105 H.M. Smith: International time and frequency coordination, Proc. IEEE **60**(5), 479–487 (1972)
5.106 H.M. Smith: International coordination and atomic time, Vistas Astron. **28**(1), 123–128 (1985)
5.107 T.J. Quinn: The BIPM and the accurate measurement of time, Proc. IEEE **79**(7), 894–905 (1991)
5.108 P. Tavella, C. Thomas: Comparative study of time scale algorithms, Metrologia **28**, 57–63 (1991)

5.109 C. Audoin, B. Guinot: *The Measurement of Time* (Cambridge Univ. Press, Cambridge 2001)
5.110 ITU: Time scales. In: *Handbook Satellite Time and Frequency Transfer and Dissemination* (ITU, Geneva 2010) pp. 78–91
5.111 B. Guinot: Some properties of algorithms for atomic time scales, Metrologia **24**(4), 195 (1987)
5.112 R.A. Nelson, D.D. McCarthy, S. Malys, J. Levine, B. Guinot, H.F. Fliegel, R.L. Beard, T.R. Bartholomew: The leap second: Its history and possible future, Metrologia **38**, 509–529 (2001)
5.113 ITU: *Standard-Frequency and Time-Signal Emissions, ITU-R Recommendation TF.460-6* (ITU, Geneva 2002)
5.114 BIPM: Values of the differences between UTC and its local representations by individual time laboratories (Bureau International des Poids et Measure, Sèvres 2016) ftp://ftp2.bipm.org/pub/tai/publication/utclab/
5.115 ITU: *Time-Scale Notation, ITU-R Recommendation TF.536-2* (ITU, Geneva 2003)
5.116 C. Han, Z. Cai, Y. Lin, L. Liu, S. Xiao, L. Zhu, X. Wang: Time synchronization and performance of BeiDou satellite clocks in orbit, Int. J. Navig. Obs. **371450**, 1–5 (2013)
5.117 K.R. Brown: The theory of the GPS composite clock, Proc. ION GPS 1991, Albuquerque (1991) pp. 223–241
5.118 A.L. Satin, C.T. Leondes: Ensembling clocks of the Global Positioning System (GPS), IEEE Trans. Aerosp. Electron. Syst. **26**(1), 84–87 (1990)
5.119 K. Senior, P. Koppang, J. Ray: Developing an IGS time scale, IEEE Trans. Ultrason. Ferroelectr. Freq. Contr. **50**, 585–593 (2003)
5.120 J. Ray, K. Senior: IGS/BIPM pilot project: GPS carrier phase for time/frequency transfer and timescale formation, Metrologia **40**, S270–S288 (2003)
5.121 K. Senior: Report of the IGS working group on clock products, 19th Meet. Consult. Comm. Time Freq. Sèvres (BIPM, Sèvres 2012) pp. 219–236